DEFORMATION IN THE PRESENCE

OF FLUIDS AND MINERAL REACTIONS:

Effect of Fracturing and Fluid-rock Interaction on Seismic Cycles

J.-P. Gratier[1] and F. Gueydan[2]

In: The Dynamics of Fault Zones, edited by M.R. Handy, G. Hirth, N. Hovius, *Dahlem Conferences, vol. **95**,*
The MIT Press, Cambridge, Mass., USA

[1] LGIT, CNRS-Observatoire, Geosciences, Rue de la Piscine, Université Joseph Fourier, 38 041 GRENOBLE, France
[2] Geosciences Rennes, Université Rennes 1, Bat 15, Campus de Beaulieu, 35042, RENNES, France

ABSTRACT

Natural and experimental deformation of fault rocks show that fluid flow and mineral reactions are linked to fracturing in a non-linear feedback relationship that potentially affects the displacement- and stress-histories of large faults. These interactions spawn instabilities that are expressed as episodic seismic events involving cataclasis which alternate with slow, aseismic deformation involving pressure-solution creep, as well as healing and sealing by fluid-assisted mass transfer. This paper focuses on the time scale of these processes during the earthquake cycle, with special emphasis on the evolution of rheological and transport properties of fault rock during the interseismic period. Fracturing weakens faults dramatically by enhancing the kinetics of pressure-solution creep and of mineral reactions. Therefore, during the post-seismic period and initial part of the interseismic period, weakening is faster than fault strengthening by healing and sealing of fractures. During the interseismic period, mass transfer associated with fluid-assisted chemical reactions smooths asperities on fault surfaces, heals fractures and enhances the formation of a foliation parallel to the fault plane. Sealing the pore space in faults also decreases permeability, and if advective fluid inflow is significant, this can increase pore-fluid pressure and reduce effective shear strength, at least locally within the fault. In the long term, however, the combined effect of fracturing, pressure-solution creep and sealing is to restore the rheological and transport properties of the fault during the interseismic period, setting the stage for renewed stress build-up and seismicity. We demonstrate the salient characteristics of fluid-assisted fault weakening and -strengthening with a 1D model of an idealized fault zone undergoing simple shear at constant velocity. The model shows that the kinetics of the weakening and strengthening processes determines the relative rates of shear stress decrease and increase during the interseismic period. The kinetics of dissolution precipitation and mineral reactions are therefore expected to be an important control on the recurrence time of earthquakes.

1 – INTRODUCTION

Several lines of evidence show that fluids play a key role in the dynamics of faulting. Fluids are preserved as fluid inclusions in minerals that grew in fault zones. The isotopic composition of such fluids reveals various origins: meteoric fluids, and metamorphic fluids produced by chemical reactions in the lower crust or mantle (Hickman et al., 1995). In some cases, cyclical fault cementation (e.g., Stel, 1981) betrays transient flow along paths which episodically opened by critical fracturing and closed by crystal growth and compaction processes. The presence of reactive fluids is also crucial in accommodating deformation by mass transfer in solution. Pressure solution is the main mechanism competing with cataclasis in the upper crust (Fig. 1a).

Both mechanisms are well documented in exhumed natural fault rocks. In the upper crust, deformation accommodated by mass transfer in a solution does not require high differential stresses. However, chemical reactions in a non-hydrostatic stress field are generally very slow, resulting in strain rates ranging from 10^{-11} to 10^{-15} s^{-1} , Rutter (1976), Pfiffner and Ramsay (1982). Reproducing such low strain rates in the presence of a fluid in the laboratory is therefore a challenge (Paterson, 2001). In contrast, cataclasis can be very fast (strain rates of 10^{-2} to 10^{0} s^{-1}). Such rates are reproducible in the lab, but require much higher differential stresses. Neither mechanism is very sensitive to temperature and they tend to become subordinate to thermally activated creep at depths greater than 10-15 km (Fig. 1a).

Cataclasis and deformation by diffusive mass transfer are not mutually independent processes. Their interaction leads to complex behaviour both in time and in space. Both mechanisms affect weakening and strengthening, but their characteristic times are very different (Group 1 report, Furlong et al., 2005, this volume). It is convenient to distinguish three characteristic times for the evolution of the mechanical properties of fault rocks:

Seconds to minutes are characteristic of cataclastic failure associated with earthquakes. The role of fluids during such short intervals is mostly mechanical (due to change of fluid pressure associated with fluid advection) or catalytic (melting).

Tens to thousands of years is characteristic for the evolution of the rheological and transport properties of rock during the interseismic period (Group 2 report, Tullis et al., 2005, this volume). In this paper, we focus on the role of fracturing and fluid-rock interactions within this time interval because these processes are key in the weakening and strengthening of faults in the upper crust. In the following, we show how fracturing speeds up the kinetics of pressure solution creep and mineral reaction, leading to dramatic weakening as well as to progressive healing and strengthening of fault. To demonstrate these effects we present some simple models which explain how the duration of the interseismic period, and thus the recurrence time of large earthquakes, is directly related to the kinetics of fluid-rock interaction.

Thousand to millions of years is the characteristic time of chemical and mechanical differentiation processes associated with mass transfer, see for example Robin (1979). The deformation of natural polymineralic rocks leads to chemical and mechanical differentiation at all scales, from a few microns to several kilometers (Gratier, 1987). For example, fault zones develop into narrow weakened gouge between progressively strengthened damage zones (Fig. 1b) see for example Evans and Chester (1995). Long-term weakening associated with reactive mass transfer (Wintsch et al., 1995) is also responsible for the formation of ductile shear zones (Fig 1c). The duration of strain localization in ductile shear zones is crudely estimated to range anywhere from a few thousand years (Handy, 1989) to tens of millions years (Muller et al., 2000). Placing tighter constraints on the rates of weakening and localization awaits the development of new analytical techniques to date fabric associated with syn-tectonic mineralization events (Person et al., 2005, this volume).

2- FRACTURING AND FLUID – ROCK INTERACTIONS

2 - 1 – BASIC CONCEPTS

Thermodynamics: the driving forces

Stress affects the chemical potential of a solid by increasing both its molar free energy and surface chemical potential compared to that at zero stress (Gibbs, 1877; Paterson, 1973). Though Gibbs free energy is not defined for a non-hydrostatically stressed solid, dissolution and precipitation of a solid is commonly described by the surface chemical potential:

$$\Delta\mu = \Delta f + V_s \Delta\sigma_n + \Delta E_s \qquad (1)$$

where μ is the chemical potential of the dissolved component, σ_n is the normal stress component or the fluid pressure P on the solid, f is the molar Helmholtz free energy, V_s is the molar volume of the solid, E_s is the surface energy : $\gamma V_s (1/r + 1/R)$, with γ interfacial energy, *r* and R principal radii of curvature (Kingery et al., 1976). Relationship (1) characterizes the chemical potential of the solid at each point on the mineral surface. This potential varies from the contact surface (σ_n) to the pore surface (P_f) in Figure 2a. The driving force for material transfer along a grain surface is therefore the difference in chemical potentials at the stressed and un- or less-stressed surfaces. The term Δf contains various contributions (Paterson, 1973):

$$\Delta f = \Delta E_e + \Delta E_p \qquad (2)$$

where E_e is the elastic strain energy, E_p is the plastic strain energy due to dislocations.

The driving force linked to the difference of surface curvature ΔE_s, sometimes called the coarsing potential (Ostwall ripening), includes both the effect of the small particles trapped in the crack and the change in surface curvature of the crack (including changes induced by crack healing). The effect of the difference in normal stresses is most often one or two orders of magnitude greater that of other effects (Paterson, 1973; Lehner, 1995; Shimizu, 1995). However, in cases when the normal stress does not vary along the solid surface (e.g., in cavities under pressure), each of the contributions to Δf and ΔE_s may drive mass transfer. For example , ΔE_s is the driving force associated with self-healing of the crack (Brantley et al., 1990), ΔE_e and/or ΔE_p are responsible for local dissolution near the boundary of an indenter, as e.g., in the knife-edge experiment of Tada and Siever (1986).

Kinetics: the limiting processes

Pressure solution is a sequence of three processes: dissolution, mass transfer and redeposition. The slowest of these processes imposes its kinetics on the whole deformation process and is termed the rate limiting step or process. Various creep equations may be written according to which process is rate-limiting, an approach which we have summarized briefly below. However, when the kinetics of the three

processes are very similar, the driving force is partitioned subequally between these processes, leading to a relatively complex equation (Raj, 1982).

Mass transfer in Nature may occur both by diffusion or by advection, although generally advective fluid flow is more competitive at longer length scales (hm to km), as discussed in Yardley & Baumgartner (2005, this volume). We do not discuss here in detail the various creep laws based on the assumptions above (e.g., Paterson, 2001). If only the driving force for pressure solution is the difference in normal stress between contacting and free surfaces, then for simplicity, creep laws for the deformation of a rock cube in a closed system take the form of equations 3 to 5 below:

(R) $\dot{\varepsilon} = \alpha\, k\, c\, V_s\, (\Delta\sigma_n)^n / R\, T\, d$ (3)

if dissolution or crystallization are the rate-limiting processes (Raj, 1982)

(D) $\dot{\varepsilon} = \beta\, D\, w\, c\, V_s (\Delta\sigma_n)^n / R\, T\, d^3$ (4)

if diffusion through a fluid phase under stress is the rate-limiting process (Rutter, 1976)

and

(I) $\dot{\varepsilon} = \lambda K\, \Delta c\, \Delta h / \Delta x\, d$ (5)

if advection through a porous aggregate is the rate-limiting process (Gratier and Gamond, 1990). In all three equations above, $\dot{\varepsilon}$ is the axial strain rate ($\Delta d/d\Delta t$), α, β, λ are dimensionless constants that depend on the geometry of the interface, d is the length of one side of the deforming cube and corresponds to the size of the closed system for mass transfer (Fig. 2b, model R and D; Fig. 2c, model R and I), t is time, k is the rate of reaction, c is the concentration of solid in solution (models R and D, volumetric ratio), V_s is the molar volume of the stressed solid, Δ (model I and Fig. 2c) is the difference in concentration of the solid in solution between the zone of dissolution (fluid-mineral interaction through the entire cube of rock) and the zone of deposition (sealed fracture). R is the gas constant, T is temperature in °K, K is the permeability coefficient, and $\Delta h/\Delta x$ is the head gradient that drives advective transport.

Three principal models can describe the stressed fluid phase: (1) the thin-fluid film model (Weyl, 1959; Rutter, 1976); (2) the island-channel model (Raj, 1982; Spiers and Schutjens, 1990); and (3) the microcracking model (Gratz, 1991; den Brok, 1998). Here, we consider a thin-fluid model with diffusion coefficient, D, and thickness of the fluid phase, w, subjected to normal stress, σ_n. The stress exponent, n, is 1 in most pressure-solution creep laws. However, for several reasons this is only true to a first approximation:

- The difference in solubility of the solid between the zone of dissolution and the zone of deposition depends exponentially on the chemical potential (Dewers and Ortoleva, 1990).

- When diffusion is rate-controlling and maintains the balance of the diffusive flux out of the fluid film, the normal stress at the center of the contact must be higher than the average stress across the contact (Weyl, 1959; Rutter, 1976). In this situation, a linear strain-rate versus stress relation is only predicted at stress values of $\Delta\sigma_n$ less than 30 MPa.

- Finally, when dissolution or precipitation is rate-controlling, n reflects the magnitude of the interface velocity versus the driving force relation and is typically 2 for spiral growth/dissolution (2D nucleation or dissolution on surfaces that are smooth and flat on the atomic scale) and 1 for a rough interface (evolution without a layer-to-layer mechanism of growth or dissolution), Niemeijer et al. (2002). Indentation experiments on quartz (Fig. 3a) confirm this complex non-linear behavior. For example, an experimental curve $\Delta l/\Delta t = f(\Delta\sigma_n)^n$ can be fitted by a power law with exponent, n, ranging from 1.3 to 2 (Gratier, unpublished results).

Other creep laws are possible, with each step potentially being a rate-limiting step. Crystallization must also be considered as a possible rate-limiting step, either due to coating of the depositional surface or to the small surface area available for precipitation. In the latter case, crystallization must occur under stress. This is the so-called “force of crystallization“ concept that was reproduced experimentally by Taber (1916) and rarely discussed since (Weyl, 1959; Means and Li, 2001; Hilgers et al., 2004).

These various creep laws (equations 3, 4, 5 and others) operate over a large range of conditions. The most important parameters controlling the relative activity of the mechanisms in these models are strain rate, size of the closed systems, temperature and nature of solids and fluids:

- For example, pressure solution of quartz is controlled by reaction-rate at low temperature and by diffusion-rate at high temperature (Oelkers et al., 1996; Renard et al., 1997).

- Nature of solids and fluids is also a key factor as, for example, the effect of pore fluid impurity ions that slow the reaction rate (Zhang et al., 2002) and consequently favour reaction control on mass transfer rates in some natural systems.

- Special attention should be paid to the relationship between strain rate, $\dot{\varepsilon}$, and the size of the closed system, d, which varies from 1/d for the I and R laws, to $1/d^3$ for the D law.

- The size of the closed system also differs depending on the mass transfer process: micrometer to decimeter for diffusion transfer (model D) compared to hundreds to thousands of meters for advection transfer (model I, see also Yardley and Baumgartner, 2005, this volume).

Evaluating the validity of the creep laws above under natural conditions is not easy. The characteristic times for diffusion, transport and precipitation on a given length scale are several

orders of magnitude longer than the human life span. Therefore, the kinetics of these processes in the laboratory must be accelerated so that experimentalists can outlive their experiments. This can be achieved in one of several ways, each with its attendant problems:

- Solubility can be increased, but not without inducing possible chemical side effects.
- Temperature can be increased but only at the risk of favouring solid-state creep mechanisms with a higher activation energy than that of pressure solution (e.g., Nabarro-Herring creep, a mechanism which is otherwise unlikely to operate in fault rocks, Rutter, 1983).
- Stress can be increased at the risk of inducing intracrystalline plasticity (dislocation glide plus -climb) or cataclasis.

Taken together, these problems raise the question of how to model the rheological behaviour of large volumes of rock with constitutive equations that are derived only from laboratory specimens at unnaturally high strain rates. Possible solutions to the problem of scaling are discussed by Paterson (2001) and touched on by Handy et al. (2005, this volume).

2 – 2 – FAULT WEAKENING

Observations from both experiments and nature show that microfracturing of minerals can drastically increase the kinetics of pressure solution. Because microfracturing occurs suddenly, pressure solution can favours transient creep.

2 – 2 – 1 Evidence from experiments

A sketch of the experimental set-up is shown in Figure 3a. A stainless steel cylindrical indenter is mounted beneath a Teflon piston in contact with a crystal of halite in its brine. Before the indenter is placed in contact with the sample, the crystal is immersed in brine that was previously saturated with halite powder at the temperature of the experiment. This is done to trap a saturated fluid phase beneath the indenter before the indenter exerts stress. In this example, the dead weight induces a stress of about 16 MPa on the indenter. The device was maintained at a temperature of 25°C. For the 150 days duration of the experiment, the displacement of the indenter was registered by following a reference line on the piston under a microscope (Fig. 3b). The result was rather surprising. The displacement-rate of the indenter was constant for the first 71 days (less than 1 micron per day) before suddenly accelerating by a factor of 8. This increased displacement-rate value persisted for the remaining 77 days of the experiment. After the sample was polished, the depth of the hole created by dissolution of the halite beneath the indenter matched the measured displacement (Fig. 3c). Other than this cylindrical hole, the only change in the structure of the sample occurred on day 71, when the displacement-rate suddenly increased: radial fractures developed in the halite beneath the indenter, as seen in Figure 3c.

Other experiments have been conducted with a similar set-up (Hickman and Evans, 1991, 1995; de Meer et al., 2002; Dysthe et al., 2003), but so far, this is the only experiment in which fractures developed during indentation. The effect of fracturing on the displacement-rate is obvious and irreversible. We interpreted fracturing to have augmented the rate of diffusive mass transfer along the contact between the indenter and halite (Gratier et al., 1999). Without fracturing, the displacement-rate ($\Delta d/\Delta t$) is controlled by the rate of mass transfer out of the thin fluid film trapped beneath the indenter, and is inversely proportional to the square of the diameter, d, of the indenter (model D, equation 4). Within this trapped fluid phase (Fig. 3b, before fracturing), the product D.w ($m^3\ s^{-1}$) is about $5\ 10^{-19}\ m^3\ s^{-1}$, in good agreement with values from previous work (Hickman and Evans, 1995; de Meer et al., 2002). Radial fractures that are longer than the diameter of the indenter and several microns wide form paths for fast mass transfer away from the indenter contact area. Along these new paths, diffusive mass transfer occurs within the free fluid that fills the open fractures. There, the product of the diffusion coefficient ($2\ 10^{-9}\ m^2\ s^{-1}$) and the width of the mass transfer path ($2\ 10^{-6}$ m) is about $4\ 10^{-15}\ m^3\ s^{-1}$, that is, about $8\ 10^3$ higher than within the thin fluid phase otherwise trapped beneath the indenter. After fracturing, the initially thin fluid film is distributed among several smaller domains, with each domain being bounded by fast diffusive paths (Fig. 3e). Therefore, fracturing renders the displacement rate inversely proportional to the square of the mean size of the small domains bounded by the radial fractures. This explains the sudden increase of the displacement rate, as pressure solution indentation is diffusion-controlled. The ratio between the indenter diameter and the mean size of the fractured domains is about 2.8.

A significant increase in the rate of pressure solution has been attributed previously to subcritical microcrack growth (Gratz, 1991; den Brok, 1998) at grain-boundaries, where channels along closely spaced microcracks intersect the dissolution surface. The location of these channels changes continuously as microcracking progresses (dynamic channel island model). Therefore, microcracking and its effects on diffusivity are considered to be integral parts of steady-state pressure solution creep.

In contrast, our model proposes that unsteady creep occurs because fracturing is able to connect the fluid phase under stress with the free fluid that located around the contact. This short-cut of the diffusional mass transfer path is responsible for the sudden increase of the creep rate. We suggest that transgranular fracturing during earthquakes

drastically enhances pressure solution and weakens rocks after the seismic events.

Fluid-filled microfractures that potentially act as short-cuts in the diffusional path have also been proposed to account for high rates of measured diffusion (Farver and Yund, 1999). However, fast healing may alleviate such short-cuts. Note that at the conditions of our experiment the fractures do not heal, they remain open paths of fast diffusion throughout the experiment. However, healing and sealing are very common processes in both experimental and natural deformation and strength recovery is a key process that competes with dissolution. This will be discussed in the following section in the context of fault healing and strengthening.

2 – 2 – 2 Applications to Nature

Fractured grains or pebbles

The idea that fracturing enhances pressure solution has several applications in natural deformation. Pitted pebbles have long been attributed to pressure solution (Sorby, 1865; McEwen, 1978, Fig. 3d). However, the large size of the dissolution areas (cm) is incompatible with the known duration of the deformation and is certainly inconsistent with experimentally derived parameters for pressure solution. Only the development of fractures at stressed contacts explains the relatively high strain rate inferred for the large pits. A numerical model (Gratier et al., 1999) of the complex interaction between pressure solution and fracture development explains why these two mechanisms are so often associated in Nature. For example, a cyclic stress time function at constant displacement-rate is derived by taking into account the ratio of stress to the diameter of dissolution (σ/d^2). Without any fracture, the contact area increases and stress must increase in order to maintain a constant displacement-rate. However, stress cannot increase infinitely, otherwise the pebble will fracture. If fracturing does occur, then the dissolution contact area is broken up into smaller domains, reducing the mean distance of diffusion that controls the kinetics of mass transfer (Fig. 3f). Therefore, the stress needed to maintain a constant displacement rate is drastically reduced. This model yields a mean viscosity of 3 10^{21} Pa.s, but the viscosity and the stress values evolve with time (Fig. 3f).

Fracturing and reaction-weakening

Reaction-weakening assisted by micro-fracturing and diffusive mass transport in fluids is common during shear zone formation in the lithosphere (Wintsch et al., 1995; Handy and Stunitz, 2002). Reaction-weakening involves the nucleation and growth of a reaction product that is weaker than the reactants. Fracturing creates the space necessary for the infiltration of fluids that are required for the reaction to take place. Figure 4 shows three examples described below:

1- Midcrustal shear zones often consist of fine-grained mylonites within granitoid host rocks typical of continental crust (review in Fitz Gerald and Stünitz, 1993). At greenschist facies conditions (depths of 10 - 20 km), quartz deforms predominantly by dislocation creep while feldspar fractures (Simpson, 1985). The transformation of feldspar to very fine-grained white micas, albite and clinozoisite is inferred to weaken the rocks in the shear zones formed at these depths (e.g. Mitra, 1978; White and Knipe, 1978; Dixon and Williams, 1983; Gapais, 1989; Wibberley, 1999). Evidence for coeval syntectonic feldspar fracturing and reaction-weakening is inferred to have occurred within the Tenda Shear Zone of Eastern Corsica (Gueydan et al., 2003; Fig. 4). This shear zones affects granitoids that can be considered as homogeneous at regional scale. We will not discuss here in detail the processes of mechanical instabilities (see Handy et al., 2005 this volume). The modal amount of white mica increases with strain and reaches a maximum value of 50%. At midcrustal depths, the transformation of feldspar to white mica requires the addition of water. The formation of fine-grained white mica weakens the material and so favours strain localization within meter- to kilometer-wide shear zones.

2- Handy and Stünitz (2002) showed that fracturing and reaction weakening are responsible for the formation of shear zones in the upper part of the lithospheric mantle during Early Mesozoic rifting of the Apulian continental margin. During extensional unroofing of these mantle rocks, fracturing triggered the progressive replacement of olivine-cpx-opx and spinel by a hydrous lower pressure assemblage of olivine + plagioclase + hornblende. This reaction, which required fracturing and fluids, weakened the material by at least an order of magnitude (stage 1, Fig. 4) as inferred from microstructural evidence for viscous granular flow probably accommodated by diffusional mass transfer along grain boundaries of the very fine-grained syntectonic reaction products. The upper mantle was thus inferred to evolve from a high-strength layer into a low viscosity detachment layer that accommodated significant extensional deformation within the rifted margin.

3- The transformation of granulite to eclogite also involves the fracturing, fluid flux and syntectonic reaction, and is inferred to have induced pronounced weakening and strain localization. Klaper (1990), Austrheim and Boundy (1994) and Jolivet et al. (in press) showed that during Caledonian subduction of nominally dry granulites rock in the Western Gneiss Region (Norway), metamorphic reactions were delayed until fracturing allowed fluid infiltration. The occurrence of pseudotachylites in some of these eclogitized fractures indicates that embrittlement was seismic and localized subsequent ductile deformation.

Eclogitization was in fact spurred by further deformation and fluid infiltration, resulting in the formation of isolated blocks of granulite separated by eclogite shear zones. These blocks are inferred to have behaved like rigid inclusions between the shear zones.

Dissolution around a fault

To accommodate large displacements, the country rock between and adjacent to faults must undergo internal deformation. This deformation is a geometrical necessity near the termination of a fault or at compressive and tensile bridges linking fault arrays. On a much smaller scale, deformation also occurs around asperities on the fault planes (Fig. 1b). Exhumed fault segments of various seismically active faults in California reveal that pressure solution is clearly associated with fracturing through the entire thickness of the upper crust: at shallow depths, calcite is more mobile than quartz, whereas the reverse is true at greater depth (Gratier et al., 2003). These authors suggested that coseismic microfracturing enhances pressure solution creep and may explain post-seismic creep. Transient values of viscosity are expected to be high during post-seismic creep, certainly greater than the mean viscosity values typical of interseismic creep (Hickman et al., 1995; Person et al., 2005, this volume). For example, in the same region, carbonate-rich rocks deformed at about 2 km depth within the Little Pine fault zone (California) yield strain values of 30%, and reasonable estimates of the differential stress (20 MPa) and the duration of deformation (4 Ma) indicate that the mean viscosity was about 8 10^{21} Pa.s. Modelled values of effective post-seismic viscosity have been evaluated assuming pressure solution of calcite in the upper part of the crust and of quartz in the lower part (see Fig. 8f). Post-seismic viscosity is strongly dependent on the fracture density, which is not easy to evaluate. However, for a mean fracture spacing associated with each seismic episode of 200 microns, and using the creep equations above (Renard et al., 2000) the effective viscosity just after the earthquake may have been about 6 10^{18} Pa.s (Gratier et al., 2003).

As cracks and fluid advection paths evolve with time, and fractures are progressively sealed, the evolution of viscosity is more complex. In fact, it probably decreases exponentially with time according to the relation of Renard et al. (2000), as explain below in more detail. Geological strain-rates in active fault zones reflect cyclic fracturing, fluid fluxes and reaction (Knipe and Wintsch, 1985). Pressure-solution creep enhanced by microfracturing may account for some examples of aseismic displacement registered by continuously operated GPS stations arrayed on active faults (Bokelmann and Kovach, 2003).

Finally, it must be noted that dissolution in polymineralic rocks can lead to the development of tectonic layering (e.g. solution cleavage) that initiates perpendicular to the direction of maximum stress when layers with soluble phases are selectively dissolved and leave the rock (Cosgrove, 1976; de Boer 1977; Robin, 1978; Gratier, 1987). Fletcher and Pollard (1981) have modelled this evolution as the propagation of a zone of negative dilation (a so-called "anti-crack") around weak or depleted inclusions. Nucleation and growth of platy mineral (micas) perpendicular to the direction of maximum stress reinforce the schistosity. The progressive development of a mechanical anisotropy, that can rotate during shearing, affects the rheological and transfer properties of fault rocks.

Dissolution of faults asperities

As the fault surface is irregular, asperities hindering displacement can also change shape by stress-induced dissolution (Figs. 5a, b). In Fig. 5d, dissolution occurs on the surface that prevents sliding (for simplicity the surface is oriented perpendicular to the maximum stress), whereas deposition occurs in the void created by aseismic fault displacement. This in turn leads to the formation of mineral fibers on fault surfaces (Figs. 5a, b, Gratier and Gamond, 1990). The dissolution of asperities may reduce fault strength. The frictional shear strength of the fault is considered here to be the yield stress needed to fracture a large part of the fault. Its shear strength may be considered to be proportional to the cumulative length of the asperities along the fault. If the total length of asperities decreases due to their progressive dissolution, the frictional shear strength of the entire fault decreases with time. The rate of this weakening can be expressed as the relationship between the rate of dissolution and the length of the asperities. The theoretical relations described above for the different rate-limiting processes (equation 3, 4, 5) may be used to do this. For the simple geometry adopted in Fig. 5d, the sliding rate, $\dot{d}$, is related to the displacement rate, $\Delta d/\Delta t$, by a numerical coefficient. In some relations (equations 3 and 5, respectively for models I and model R), the sliding rate does not depend on the distance of mass transfer, d, from dissolution to deposition zones. In the other relation (equation 4, model D), the sliding rate depends on the inverse of the square of the distance of mass transfer, d. This distance, d, is the asperity length for dissolution of only one side of the fault. Because, d, also depends on the crystal growth mechanism, it is assumed here that each growth increment occurs at the vein/wall contact. The relation between stress and the asperity length is related to the change in energy consumed during sliding to an extent dependent on the creep law. On the other hand, the energy needed to break asperities

always depends on the asperity length. Thus, the energies needed to accommodate cataclastic flow and pressure solution sliding are comparable (Figs. 5e and 5f). At the scale of a single asperity, stable sliding is expected when the two energies vary similarly (e.g. pressure solution sliding), whereas unstable sliding is expected when the two energies vary differently with successive mechanisms, thereby minimizing overall strain energy dissipation (e.g., pressure solution sliding then cataclasis). The behaviour of all asperities on a fault is more complex (e.g., see experiments by Bos et al., 2000) and needs to be modelled numerically. In any case, considering all asperities, pressure solution reduces the shear strength of the fault by progressively reducing the total length of the asperities.

A leading objective for future work will be to establish the geometrical evolution of asperities and their sliding mechanism (Nadeau and Johnson, 1998; Sammis and Rice, 1998). One way to do this is to compare the true geometry of a fault surface (Fig. 5c) with that of threaded surfaces (Thibaut et al., 1996). A threaded surface is an uneven surface that allows the sliding of two rigid blocks without any deformation (like the surfaces of bolt and nut). Deviation of real fault surfaces from that of ideally threaded surfaces may reveal the true geometry of fault asperities.

2 – 3 –FAULT STRENGTHENING

2 – 3 – 1 – Pervasive strengthening

Numerous observations of natural deformation show that deposition selectively strengthens rocks. For example, quartz and calcite mineral deposits in pressure shadows of stronger minerals indent their slaty matrix by developing dissolution haloes (Fig. 6a). Another example is “bamboo-like structures“ created by boudins that selectively strengthened the boudinaged layer (Fig. 6b). The same behavior was observed in experimentally deformed polymineralic aggregates with soluble and insoluble minerals (Zubtsov et al., 2004). At room temperature, the compaction rate of a polymineralic aggregate was significantly higher than that of a monomineralic rock comprising only a single soluble species. This may reflect the fact that the grains of monomineralic rocks grew together rather that dissolving under stress. The presence of another mineral phase favors dissolution along mutual contacts between phases with contrasting solubilities. Hickmann and Evans (1991) also found that dissolution at halite/silica interfaces (silica being insoluble) was much faster than at halite/halite interfaces, which tended to grow together. In all the natural examples (Figs. 4 and 6), strengthening linked to mineral precipitation competed with weakening linked to the concentration of less-soluble micas. Deformation with mass transfer leads to a progressive segregation of rocks that induces rock heterogeneities (mass transfer from weakened zones of dissolution to strengthened zone of deposition). Therefore, rock viscosity evolves with space and time with viscosity contrasts generally increasing to an extent dependent on the size of the closed system. The size of this closed system, and the characteristic size of the induced heterogeneities mostly depend on the mechanism and scale of mass transfer: diffusion on length scales of microns to decimeters size (e.g. tectonic layering) or advection on scales of hundred to thousands of meters (e.g. ore deposit).

An atypical example where the degrees of strengthening and weakening are comparable comes from silicic volcanics of Vendée (France) affected by fluid-assisted deformation (Le Hébel et al., 2002). Deformation of the quartz-Kfeldspar-phengite volcanic rock (Fig. 6c) occurred at about 400°C and 4-5 kb. The deformation involved diffusion-driven dissolution-crystallization of quartz and feldspar, with the phengite behaving as a residual, relatively insoluble phase. Increasing strain is marked by the development of alternating mica-enriched layers (sources) and quartz-feldspar (sinks), as shown in Figure 6d. The former are expected to have weakened as mica content incresed, whereas the latter underwent microcracking (Fig 6e). This process partitions strain, with very limited localization in the micaceous layers. Recent isotopic analysis revealed limited fluid-rock ratios, showing that the fluid originated locally and that the system remained closed during ductile deformation. No transient fluids fluxes induced by microcracking were discerned. The stability of K-feldspar is consistent with the absence of external fluids under greenschist facies conditions. This is a case study where the absence of transient fluid fluxes precludes weakening at a regional scale and favors slight strengthening as marked by numerous cracks. If the system was indeed closed, then the amount of dissolved material (qtz/Kfp) is equal to the amount of precipitated material.

This behaviour contrasts with the regional evolution of zones of quartz deposition within ore deposits. Where large amounts of quartz are transported from depth by fluid flow through active faults (Sibson et al., 1988), the zone of deposition appears to strengthen significantly at the regional scale (massive quartz deposits are harder than surrounding metamorphic country rocks).

2 – 3 – 2 Fault healing and sealing

Evidence for post-seismic strength recovery comes from geophysical studies. For example, Li et al. (2003) described fault rocks from the Hector Mine rupture zone where P- and S-wave velocities had increased, respectively, by 0.7% -1.4% and 0.5% -1.0% between 2000 and 2001. In contrast, velocities in surrounding rocks increased by much less, indicating that the Hector Mine rupture zone healed and strengthened after the main shock, most likely as

cracks that had opened during the 1999 earthquake closed up again and were sealed. The recovery of fault-zone strength is consistent with a decrease in apparent crack density of 1.5% within the rupture zone. The ratio of travel-time decreases for P- and S-waves was 0.72, suggesting that the cracks near the fault were partially filled with fluids. This re-strengthening is similar to that observed after the 1992 M_L 7.4 Landers earthquake some 25 km to the west (Li and Vidale, 2001).

The same observation can be made in experiments on faulted sandstones that were heated and subsequently re-deformed (Blanpied et al., 1995; Tenthorey et al., 2003). They show a strength recovery of 75% after 6h of heating at 927°C. In the most extreme case, hydrothermally induced gouge compaction, cementation and crack healing resulted in 75% strength recovery after treatment at 6h at this very high temperature. Isostatic hydrothermal treatment also resulted in dramatic reductions in porosity and permeability.

The question is thus how, and at what rate, do fractured rocks recover their strength after an earthquake ? The nature of the minerals that constitute the country rocks is very important because fluid-rock interactions play a crucial role in the rheology of fault zones. We do not consider all the possibilities here, but just cite the examples of quartz and calcite, both of which are common mobile minerals in Earth's crust. The relative mobility of quartz and calcite components clearly changes with depth due to differing pressure- and temperature dependences of their solubilities. At shallow depths, calcite is more abundant and mobile than quartz, whereas the reverse is true at greater depth. This variation is related to two effects: first, the solubility of quartz increases with increasing temperature whereas calcite solubility decreases with increasing temperature; second, at low temperature, the kinetics of quartz dissolution is very slow, precluding significant pressure solution (Oelkers et al., 1996; Renard et al., 1997). Note that the situation is probably much more complex because the temperature activation of kinetics may counteract the reverse temperature effect on the solubility, at least in the case of calcite (Rutter, 1976). Also, reaction kinetics is very sensitive to impurities in the pore fluid (Zhang et al., 2002) and this effect may outweigh effect of temperature in nature.

Various mechanisms can lead to healing, or sealing of rocks, as summarized in Figure 7. Here, we consider only the mechanisms that occur at the characteristic time of interseismic periods. Changes of fluid pressure that occur during, or just after, the main rupture with their mechanical consequences (i.e. dilational hardening, triggering of earthquakes) are discussed elsewhere (e.g., Miller, 2002; Miller et al., 2003; group 4 report, Person et al., 2005, this volume).

Based on observations of natural structures (Gratier et al., 2003), the following succession of crack sealing processes is expected in active fault zones during interseismic periods (Fig. 7a). Initially, an earthquake increases the overall permeability and reduces fluid pressures to near hydrostatic values within the fault zone. This favours an increase in the reaction rates for the reasons outlined above. Self-healing of the fractured minerals and some metamorphic reactions are relevant to this stage. Crack healing is driven by a decrease in microcrack surface energy (Fig. 7b-i). No input of external material is required at this point. Solid-solid contacts are required along the fracture in order to facilitate mass transfer from sites with maximum wall curvature to sites with minimum curvature (Fig 7b-i). Because diffusive transfer occurs in a free (unstressed) fluid, this process is usually probably controlled by the kinetics of the interface reaction and may be rather fast (days to weeks; Brantley et al., 1990). Evidence of this process is common in naturally deformed rocks. Also relevant to this stage are free-face metamorphic reactions that are activated by the advective inflow of fluids that are not in equilibrium with the minerals lining the fault. This could lead either to dissolution or to deposition that is potentially rather fast (days to years) in the case of reaction on free faces around pores or voids (Fig. 7b-iii). On the other hand, if dissolution occurs on a stressed surface, reaction kinetics is usually controlled by diffusion (i.e., sealing of large aperture cracks, Fig. 7b-iv).

Other reactions may progress at a slower rate. Beeler & Hickman (2004) proposed that crack closure may be controlled by the dissolution of asperities and microfractured grains that prop the fracture open (Fig. 7b-ii). This type of self-healing process is assisted by stress and requires a decrease in fluid pressure to operate effectively. A fluid pressure drop may explain the observation that dissolution pits occur in all the directions during gouge compaction (see Fig. 8b). If this drop is sufficiently rapid, for example during an earthquake, the rocks will tend to collapse. The experiments of Elias and Hajash (1992) in which grains or fractured rock are embedded in a "soft tube" show such pressure solution compaction. A decrease of the compaction rate is expected with time when diffusion is rate-controlling (Fig. 3).

The sealing of large-aperture cracks (10 µm to mm – cm, Fig. 7b-iv) combined with the large opening of the separated walls of the fracture (i.e., no contact of walls across the fracture) requires an influx of material into the cracks from outside sources. As pointed out above, long-range advective transport of dissolved solid (e.g., involving flushing by strongly overstaturated solution as shown in Fig. 7b(iii)) may contribute to fracture sealing (Fyfe et al., 1978; Etheridge et al., 1984). Inflow of supersaturated fluid is documented both by stable isotopes studies (Kennedy et al., 1997) and by observations of typical mineral reactions, for example, in fault gouge (Evans and Chester, 1995). This contributes to a decrease in porosity during the interseismic period, mainly in the gouge. However, it

has minor effects on the sealing of nearby fractured country rocks (Gratier et al., 2003).

Following initial fast sealing (e.g. by self-healing: Fig. 7-i, free-face metamorphic reactions: Fig. 7b-iii) that most often does not eliminate porosity (Fig. 7a), crack sealing involves diffusive mass transfer (e.g., Ramsay, 1980, Gratier and Gamond, 1990). Mechanism of dissolution and redeposition may be recognized directly by optical microscope, by chemical analysis, or by cathodoluminescence studies. Mass transfer is proportional to the difference in chemical potential between the zones of dissolution and deposition. Most often, soluble species are removed from grain-grain contacts (stylolites, solution cleavage) and reprecipitated in veins or voids (Weyl, 1959; Rutter, 1976; Gratier, 1987). In this case, mass transfer involves diffusion through the fluid phase trapped along the stressed contact, and can lead to the complete sealing of veins and voids (Fig. 7b-iv, upper part). Note that solution cleavage (S) and associated post-seismic crack-sealed-veins (CSV Fig. 7a), possibly in combination with subcritical fracturing (Atkinson, 1982), may accommodate part of the stress aseismically over the entire interseismic period. (see also Group 4 report, Person et al., 2005, this volume).

Compaction and crack-sealing involves two mechanisms (Figs. 7, 8): pervasive pressure solution at the grain scale in the gouge (Fig. 8b), and vein cementation associated with dissolution along stylolites in the damaged zone around the active faults (Fig. 8c, Gratier et al. 2003). Compaction modelling shows that these two mechanisms have different time scales (Renard et al., 2000). Pervasive pressure solution at the grain scale in fine-grained gouge is much faster than pressure solution along stylolites and associated precipitation in veins. For example, at five kilometers depth the time required to reduce permeability from 10% to near 0 is about a month for a fine-grained quartz gouge (10 microns) and a thousand years in a damaged zone with fractures spaced 100 microns apart. Therefore, slow stress-driven crack-sealing and compaction processes control the change of porosity and permeability at depth after an earthquake. The kinetics of the sealing process during advective fluid flow may also be very slow if diffusive mass transfer of dissolved rock through the stressed intergranular fluid is the rate-limiting step (Fig. 7b-iii, right).

Modelling of fluid transfer along active faults is possible if pressure-solution fracture sealing is combined with advective inflow of lower crust fluids (Fig. 8a). The compaction rate in the gouge (Fig. 8b) and the sealing rate in the damaged zone (Fig. 8c) can be calculated (Figs. 8d and 8e, respectively), the latter being the rate-controlling process (Gratier et al., 2003). The rate of sealing is modeled to decay exponentially with time. An example is given in Fig. 8g which shows the progressive change in fluid pressure from hydrostastic (just after the earthquake) to locally near-lithostatic. Lithostatic pressure develops at two different depth intervals: at depth due to the inflow of fluid from the lower crust, and in the upper crust where calcite is available for mass transfer and relatively fast sealing of the veins (Fig. 8f). Note that hydrothermal reactions in fault zones may lead to two competing time-dependent effects: fault-strengthening due to crack sealing and fault-weakening that arises from elevated pore pressures within a well cemented, low-permeability gouge layer (Fig 8g).

In summary, healing and sealing processes in faults may develop over a broad range of time scales, from several days (self-healing) to a thousand years (complete sealing of the veins by pressure solution and deposition). Strengthening therefore competes with weakening due to an increase in fluid pressure during progressive healing. This could help to localize the main rupture along the healed gouge and scatter the aftershocks within the strengthened damaged fault zones. Sealing restores and even increases the cohesion of the rock. Muhuri et al. (2003) argued that sealing does not necessarily change the frictional coefficient.

3 – A MODEL OF UPPER CRUSTAL FAULT STRENGTH

3.1 Rheological model

As explained above, the strength of fault zones can either decrease or increase with time. The characteristic time-scales of weakening and strengthening differ and this difference can control the rheology of active faults and thus influence the duration of seismic cycles. The simple rheological model proposed below account for these two effects, as shown schematically in Figures 9-a. The fault zone is modelled here as ductile material that involved pressure-solution creep, healing processes, and reaction softening. These ductile mechanisms are assumed to be relevant within the whole sismogenic crust, as it is suggested by the occurrence of pressure solution at all depths in the San Andreas Fault (Gratier et al., 2003). An alternative approach has been to model fault-weakening and -strengthening as due to a change in fault friction or cohesion (Miller, 2002; Miller et al., 2003; Sibson and Rowland, 2003). Since our interest is to quantify the role of weakening and strengthening processes that involves ductile deformation mechanisms, we propose that the fault zone behaves as a ductile material and the strength of the fault varies with time, leading to a temporal variation of viscosity. In contrast, the viscosity of the wall rock retains its initial value, η_0. Starting from this initial value, the viscosity within the fault zone, $\eta(t)$, varies with time as follows:

$$\eta(t) = [w(t)+s(t)]\,\eta_0 , \quad \text{with} \quad 0<w(t)<1 \text{ and } 0<s(t)<1 \qquad (6)$$

where w(t) and s(t) are the amount of weakening and strengthening, respectively. The initial and final states are defined by

Inital state : $w_0 = 1,\ s_0 = 0, \eta = \eta_0$ (7)

Final state : $\eta_\infty = [w_\infty + s_\infty]\ \eta_0$ (8)

The final value of weakening, w_∞ , is a free parameter that is set here to $w_\infty=10^{-2}$. The final amount of strengthening is such that $w_\infty + s_\infty = 1$ (i.e., no final change in the viscosity). s_∞ can thus be expressed as $s_\infty = 1- w_\infty$. Note that although $w_\infty + s_\infty =1$, $w(t) + s(t) \neq 1$ and depends on the relative amounts of weakening and strengthening. The viscosity of the fault zone thus changes with time according to the evolutions of the weakening and strengthening. We propose that the final amount of weakening and strengthening act as attractor, so that the weakening rate, $\frac{\partial w}{\partial t}$, and strengthening rate, $\frac{\partial s}{\partial t}$, are proportional to $(w(t)- w_\infty)$ and $(s(t)- s_\infty)$, respectively. We have shown in the sections above that the strain rate, $\dot{\varepsilon}$, within the fault zone controls the kinetics of weakening and strengthening such that

$$\frac{\partial w}{\partial t} = \varphi_w \dot{\varepsilon}[w_\infty - w(t)] \quad \text{and}$$

$$\frac{\partial s}{\partial t} = \varphi_s \dot{\varepsilon}[s_\infty - s(t)] \qquad (9)$$

The scalars φ_w and φ_s define the kinetics of weakening and strengthening and are free parameters. As discussed above, weakening may be triggered by microfracturing and fluid flow, leading to post-seismic stress relaxation. Subsequent strengthening is related to interseismic sealing of these fractures. In our rheological description, this initial predominance of weakening yields to the following condition: $\varphi_w > \varphi_s$.

For a constant strain rate, $\dot{\varepsilon}$, the weakening and strengthening derived from (9) become

$$w(t) = [w_0 - w_\infty] \exp(-\varphi_w \dot{\varepsilon} t) + w_\infty;\ \ s(t) = [s_0 - s_\infty] \exp(-\varphi_s \dot{\varepsilon} t) + s_\infty \quad \text{for } \dot{\varepsilon}=c^{te} \qquad (10)$$

The characteristic time for weakening, t_w, and strengthening, t_s, can thus be defined as

$$t_w = 1/(\varphi_w \dot{\varepsilon}) \quad \text{and} \quad t_s = 1/(\varphi_s \dot{\varepsilon}) \qquad (11)$$

Increasing φ_w at constant strain rate reduces the weakening time and leads to a sharper decrease in viscosity. An increase of strain rate (e.g., during strain localization) also increases the viscosity reduction (decreases t_w). This corresponds to a positive feedback between weakening and strain localization. In the same way, strengthening tends to delocalize strain.

Note that for a time of $5t_w$, the term $\exp(-\varphi_w \dot{\varepsilon} t)$ in equation (10) is equal to 0.007, indicating that by then, weakening has almost reached its final value, s_∞. The same holds for strengthening at time $5t_s$. Weakening and strengthening thus reach their final values at times

$$t_{w\_end} = 5t_w = 5/(\varphi_w \dot{\varepsilon}) \quad \text{and} \quad t_{s\_end} = 5t_s = 5/(\varphi_s \dot{\varepsilon}) \qquad (12)$$

After t_{w_end}, weakening ceases unless a new fracture resets weakening and strengthening to their initial values, as explained below. Fracturing occurs if the shear stress in the fault zone, $\tau = \eta \dot{\varepsilon} = [w(t)+s(t)]\ \eta_0\ \dot{\varepsilon}$, becomes greater than the yield stress , τ^y. The yield stress is assumed here to be constant, since gravity (and thus pressure) is disregarded in this study. As shown in Figure 8, the combined effects of advective fluid inflow and fracture sealing lead to a progressive increase of fluid pressure within the active fault, from near hydrostatic values after the earthquake to locally overpressurized zones. Consequently, the effective shear strength of the fault is expected to decrease progressively during the interseismic period (Miller, 2002; Sibson and Rowland, 2003). Overall weakening of the fault zone due to the formation of gouge within a damaged zone should result in a decrease of the yield stress, τ^y , with time. We disregard this long-term evolution and focus instead on the seismic cycle computed for a constant assumed value of the yield stress, τ^y.

The competing effects of weakening and strengthening on the evolution of fault strength are illustrated schematically in Figure 9-b, where strength and shear stress τ vary with time within the fault. After fracturing, weakening prevails and leads to a sharp decrease of the fault strength. The recovery of fault strength is achieved when strengthening becomes dominant, possibly leading to the nucleation of new seismic fractures.

The kinetics of the weakening and strengthening thus control the duration of the seismic cycle, as quantified in the following section. Note that the proposed rheological model and thus the predicted duration of the seismic cycle are fully dimensionless. In the future, quantification of the duration of weakening and strengthening in laboratory experiments and natural slip events (e.g., co-seismic and post-seismic deformation measurement) could define a characteristic time for cyclical changes in fault zone rheology. This calibration could be achieved by a detailed study in the lab of the kinetics of weakening processes (pressure-solution, reaction-softening) and strengthening processes (such as healing and sealing).

3.2 Boundary conditions and numerical scheme

The model comprises a 1D layering subjected to simple shearing. The bottom of the sheared layers in Figure 9 is fixed, while a constant velocity, V, is imposed at the top of the layers. A constant velocity is imposed in order to determine the relative roles of weakening and strengthening in the absence of any change in loading. The average strain rate within the fault zone of width L is $\dot{\varepsilon} = V/L$. Mechanical equilibrium is attained by numerical means (finite element method) using the code SARPP (SARPP, 2003). The layered structure is discretized

into 100 3-noded Lagrangian elements. The velocity v(y) is the only nodal unknown.

3.3 Variation in shear stress, strain rate and velocity

Figure 10 presents variations of shear stress at a given depth within the fault zone. The kinetics of weakening and strengthening were arbitrarily set at $\varphi_w = 10$ and $\varphi_s = 1$, respectively. The cyclic variations of shear stress are related to weakening (between points 1 and 2) and strengthening (points 2 to 3) that prevailed in the fault zone, as discussed above. Strain rate and velocity as a function of vertical position within the fault are also given in Figure 10b and c, respectively. Strain rate is homogeneous within the fault zone and the wall rock, reflecting the assumed absence of any vertical change in the material properties of our rheological model. The strain rate is uniform in the fault zone and in the wall rock at the beginning of the cycle, prior to the onset of weakening and strengthening. At the end of the weakening, the increase in strain rate of the fault is compensated by a decrease in strain rate in the wall rock in order to maintain mechanical equilibrium (uniform shear stress across the layering during simple shear). At the end of strengthening, the strain rate in the fault zone is almost equal the strain rate in the wall rock. The velocity profile (Fig. 10-c) is related to the strain rate profiles, reflecting the fact that the strain rate is the y-derivative of the velocity field, with y equal to the vertical coordinate. At points 1 and 3, the strain rate is uniform within both the fault zone and the wall rock, leading to a linear velocity profile (imposed velocities 0 and 1 at the bottom and top of the layering, respectively). At the end of weakening, the strain rate is higher in the fault zone than in the wall rock, leading to a sharper velocity gradient in the fault zone.

3.4 Duration of the seismic cycle

Figure 11 shows how shear stress in the fault zone varies with time for two sets of strengthening- and weakening-rate constants ($\varphi_s = 1$, $\varphi_w = 10$ in curve 1 and $\varphi_s = 5$, $\varphi_w = 10$ in curve 2). The width of the fault zone, L, and the velocity, V, are both set to 1, yielding an average strain rate of 1. For $\varphi_s = 1$, $\varphi_w = 10$ (curve 1, Fig. 11 and also Fig. 10) a rapid decrease in shear stress is observed after the onset of fracturing, corresponding to postseismic stress relaxation. The duration and rate of the stress decrease are governed by the kinetics of weakening. For $\varphi_w = 10$, the time at the end of weakening is of the order of 0.5 (eq. 12), presuming that the strain rate is uniform within the fault zone and equal to 1. This estimate is very close to the time when the minimum value of shear stress is attained (~0.4). Note that this time is greater than the time of the end of weakening due to the positive feedback between strain localization and weakening kinetics (eq. 10). During stress relaxation, strain rate increases significantly in the fault zone, leading to faster weakening. For times greater than 0.4, shear stress increases over a time span whose duration is controlled by the strengthening kinetics. Because the rate of strengthening is an order of magnitude less than the rate of weakening, the time necessary for shear stress to increase is much greater than the time of stress relaxation. In this case, the time when strengthening ceases is of the order of 5 ($\varphi_s = 1$ and $\dot{\varepsilon} = 1$, eq. 12). Again, this estimate is consistent with modelling where the strengthening ends at a time of around 6. This difference between estimate and numerical results is attributable to the decrease in bulk strain rate within the fault zone during strengthening (Fig. 10), leading to a decrease in the rate of strengthening (eq. 11). At the end of strengthening, the increase in shear stress is sufficient to trigger fracturing, which resets the weakening and strengthening variable to their initial values coincident with the beginning of a new cycle of stress relaxation and fault loading. Since the yield stress is constant through time, the time interval between two episodes of fracturing is constant.

The time interval between two episodes of fracturing within the fault zone defines the duration of the earthquake cycle, t_{cycle}. Note again that since the proposed rheological model is dimensionless, the predicted duration of the earthquake cycle is also dimensionless. However, that duration can be estimated for a natural fault if the rates of weakening and strengthening in that fault are known from creep and compaction laws. More specifically, because the earthquake cycle is defined by stress relaxation (during a time close to t_{w_end}, eq. 12) and stress loading (during a time close to t_{s_end}, eq. 12), the duration of the earthquake cycle is simply

$$t_{cycle} = t_{w\_end} + t_{s\_end} \approx \frac{5}{\dot{\varepsilon}}\left[\frac{1}{\varphi_w} + \frac{1}{\varphi_s}\right] \qquad (13)$$

For $\varphi_s = 1$, $\varphi_w = 10$, this earthquake cycle time is about 5.1. This estimate is very close to the numerical results (curve 1, Fig. 11). Increasing φ_s to 5 at the same φ_w (curve 2, Fig. 11) yields a smaller earthquake cycle time (t_{cycle}=1.5). Note also that this shorter cycle time coincides with a decrease in the shear stress drop during stress relaxation. This reflects the fact that increasing the rate of strengthening causes strengthening to dominate the strength evolution of the fault zone earlier in the earthquake cycle. Weakening prevails during a shorter time interval, leading to less pronounced stress relaxation.

In summary, the rheology of the fault zone controls the timing of post-seismic stress relaxation and interseismic stress loading. The duration of the earthquake cycle is thus controlled by the relative rates of weakening and strengthening within the fault zone. Transient weakening and strengthening are activated within the fault zone immediately after

fracturing, which opens the system and induces the advective influx of fluid. Weakening is primarily related to fluid-rock interaction (reaction-softening, pressure-solution), whereas strengthening initiates when free fluids become rare and the fault zone is sealed.

3.5 The role of fault zone width

Figure 12 depicts the duration of the seismic cycle as a function of the ratio of the rates of strengthening and weakening for two values of fault zone width, L = 1 and L = 10. The duration of the seismic cycle for L = 1 is that of Fig. 11. Increasing the width of the fault zone increases the duration of the seismic cycle. Increasing L by an order of magnitude leads to a similar order-of-magnitude increased in the cycle duration. This simple relationship directly reflects the average strain rate in the fault zone, $\dot{\varepsilon} = V/L$, where V is the velocity at the fault zone boundary and L the fault zone width. For a constant V, an increase of L yields a decrease in strain rate and thus an increase in the duration of the earthquake cycle (eq. 13). If we assume that the width of the fault zone is related to its length, these results indicate that the seismic cycle of a large fault is much longer than that of a minor fault, as observed in Nature.

4 CONCLUDING REMARKS

Within the upper crust faults, ductile deformation in the presence of fluids and mineral reactions interact with fracturing processes and this interactions leads to unstable deformation, with fast, episodic (cataclastic, seismic) slip alternating with slow (mass transfer creep). At the time scale of the earthquake cycle, fracturing speeds up the kinetics of pressure solution creep and mineral reaction, thereby weakening the fault, whereas healing and sealing of fractures re-strengthen the fault zone. These deformation mechanisms accommodated by mass transfer also relax stress during the interseismic period and partly smooth asperities on fault surfaces. The effect of fracturing on the dissolution process is faster than healing and sealing of the fault, thus the weakening effect prevails just after earthquake and strengthening develops more progressively with time. Strengthening associated with fault sealing is sometimes counteracted by weakening related to a decrease in permeability and an increase in pore-fluid pressure in the fault zone. This effect is linked to the amount of fluid inflow. Consequently, the fault zone is modelled, during interseismic period, as ductile (viscous) material that first weakens just after the earthquake then progressively strengthens. Numerical modeling shows that the relative rates of weakening and strengthening control the temporal evolution of fault strength during the interseismic period, and thus the duration of the earthquake cycle.

Future research

Microstructural approach

Numerous parameters control the characteristic time of evolving mechanical and physical properties involved in the coupled weakening-strengthening effect. The kinetics of weakening and strengthening are of course the key factors in this evolution. As presented in the paper, different creep and compaction laws are possible depending on the parameters used, as mentioned in Tullis et al. (2005, this volume).

Experiments are required to establish the rate-limiting step (that determine the type of laws) and the stress/strain-rate relations. A major problem is that the characteristic time of deformation by stress-induced mass transfer is several orders of magnitude less than the average human life-span. Activation of the experiment-rate is always needed that may, at least partially, render some interpretations of experimental results rather uncertain.

Another major factor that can only be inferred from the analysis of natural fault zones is the relative contributions of advection and diffusive modes of fluid flow, and related to that, the mean distance of mass transfer within fluids (see also Yardley and Baumgartner, 2005, this volume). Careful microstructural and geochemical analysis of naturally deformed rock is required to establish this distance, which can range from the mean spacing between fractures for solution cleavage (diffusive mass transfer) to thousands meters (advection transport). Evaluating the nature of the fluid and the minerals at depth along the fault is also a crucial objective (Group 4 report, Person et al. 2005, this volume).

Multiscaling approach

We understand how individual asperities on a fault are dissolved or broken, but determining the bulk effect of asperities at all scales on bulk fault behaviour is a true challenge. A first step could be to evaluate the geometry of the asperities on exhumed fault surfaces and to consider asperities at all scales as deviations from the ideal model of a threaded surface. Another multiscaling approach needed for quantitative models is the scaling properties of fracture geometry (width, length and spacing), as these parameters play a key role in the weakening and strengthening process.

Macrostructural approach

Testing models requires regional studies of real faults. Measurements of how mechanical and physical properties (including fluid pressure) of faults zone evolve during the interseismic period are, of course, very important. In particular, monitoring of fluid pressure could be combined with geodetic measurements of fault motion (see Group 1 report,

Furlong et al., 2005, this volume) to establish the relationship between fault displacement and fluid pressure evolution along active faults. This would be especially interesting to do immediately after earthquakes, in order to capture the post-seismic creep triggered by fractures (weakening effect) then the expected links between post-seismic strengthening and the recovery of high fluid pressure. Finite displacements during aftershocks can be regarded in the broader context of long-term displacements obtained with geodetic measurements in order to constrain the post-seismic creep rate and the localization of strain along active fault zones. Fault zones with a regular earthquake recurrence time and constant displacement rate (e.g., Parkfield, southern California) lend themselves well to this kind of study, because they are expected to show a features that are diagnostic of recurrent competition of weakening and strengthening during the interseismic period.

Finally, the idea that inherited and induced heterogeneities in Nature, acting for example as a random background noise, can trigger instabilities introduces the notion of a self-organized complexity that prevents us from accurate prediction of earthquakes on useful time- and length scales (months to days, kilometers to meters). Earthquake predictions are, and will remain, beset with rather large uncertainties. Evaluating these uncertainties remains a challenge that will be enhanced by the careful study of such heterogeneities and their effects on self-organized systems.

Numerical modelling

The numerical modelling in this paper was very simple, directed as it was to exhibit the roles of weakening- and strengthening kinetics in the seismic cycle. Future modelling should account not only for changes of fault zone rheology during the earthquake cycle as proposed in this paper, but also for the change of fluid pressure. Following an earthquake, the combined effect of advective fluid inflow and fracture sealing in the fault core could lead to an increase of fluid pressure from near-hydrostatic after the earthquake to locally overpressurized, at least along some parts of the fault (see Group 4 report, Person et al. 2005, this volume, for a discussion of post-seismic fluid-pressure evolution). Consequently, the effective shear strength of the fault decreases with time during the interseismic period, indicating that the yield stress, τ^y, for fracturing decreases during this time must be implemented. Changes in yield stress are also expected to occur during the formation of gouge in the fault core, irrrespective of any changes in pore-fluid pressure. Therefore, an important step in the future would be to incorporate transient yield stress into models of the seismic cycle.

Acknowledgements:

We thank D. Gapais for his detailed comments on a previous version of the manuscript and C. Spiers, M. Handy, and J. Urai for their very helpful reviews of the final version. We also thank P. Labaume, P. Vialon and A.-M. Boullier, respectively, for the photographs in Figs. 3d, 5c and 6a.

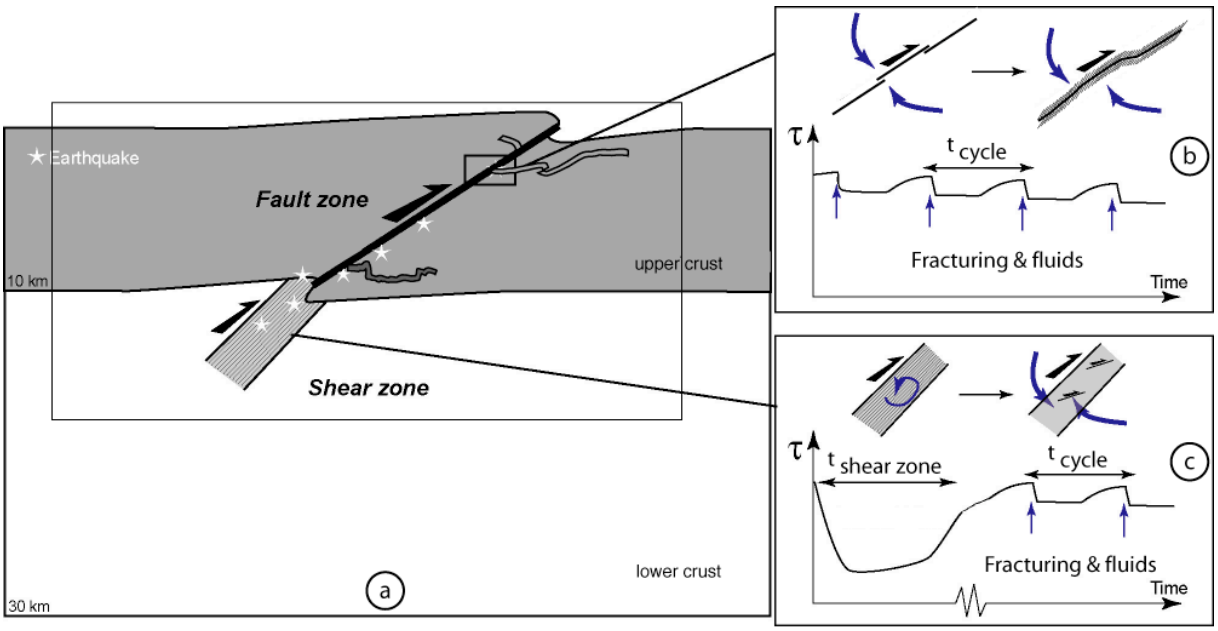

Figure 1

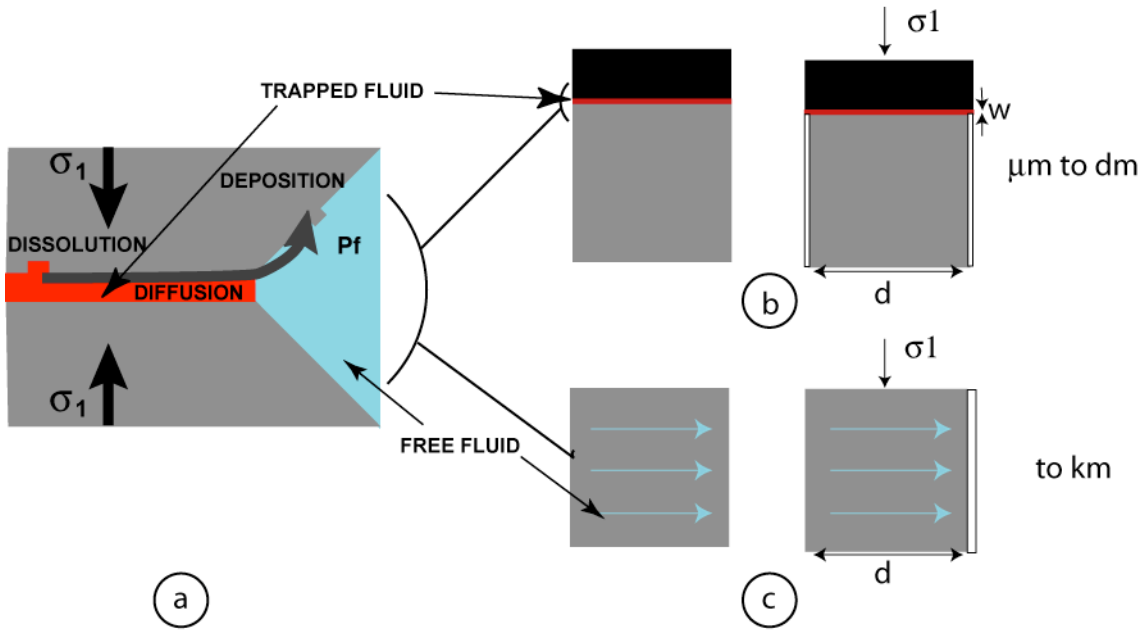

Figure 2

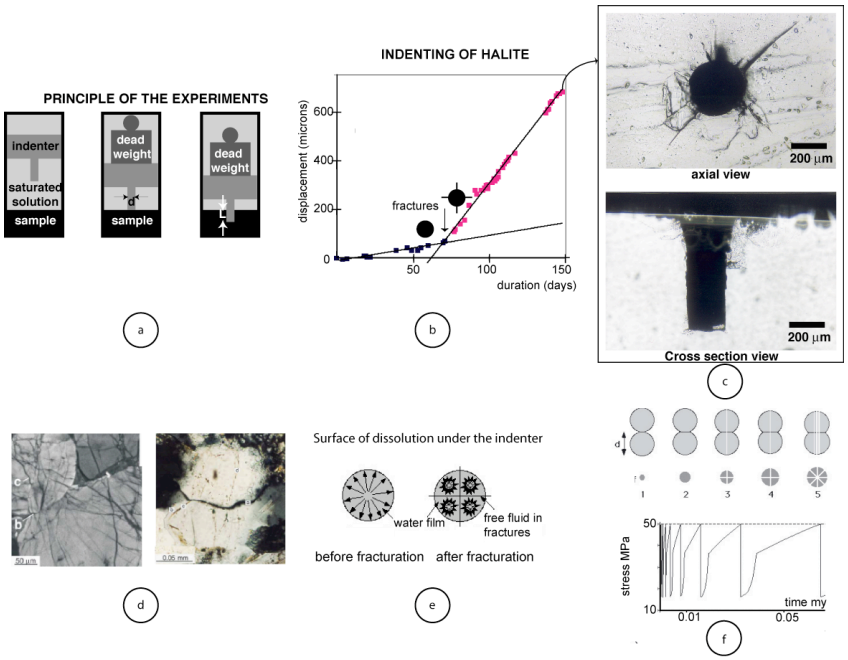

Figure 3

Fracturing and reaction-weakening (+H_2O)

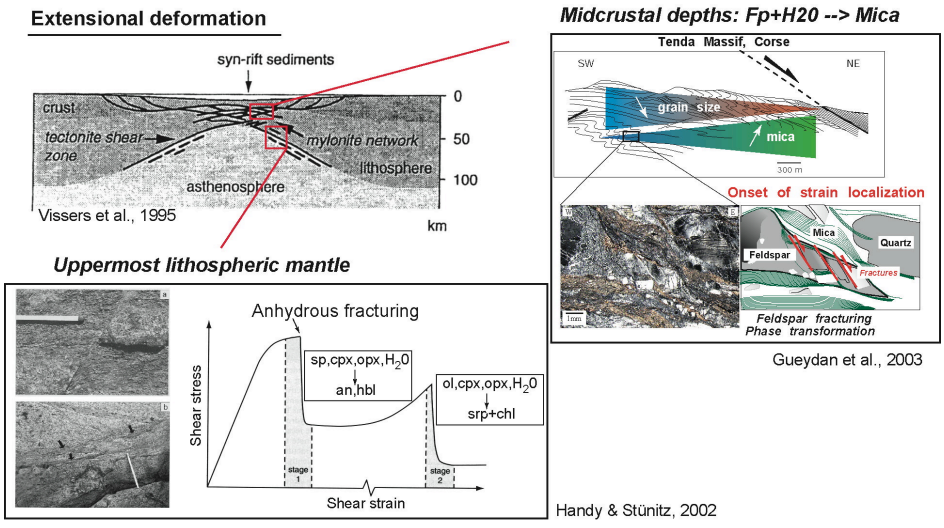

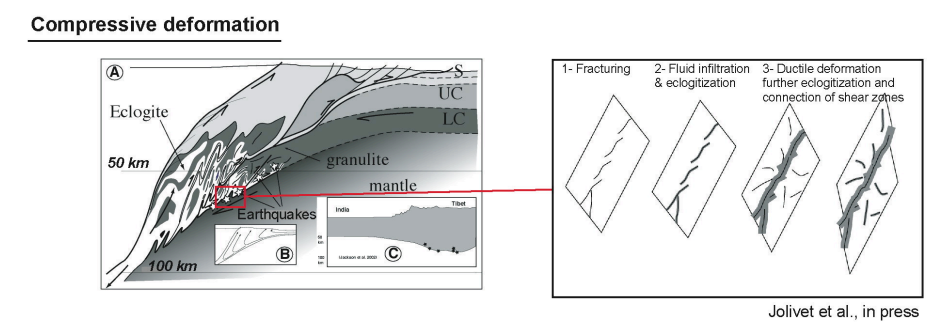

Gratier & Gueydan, Figure 4

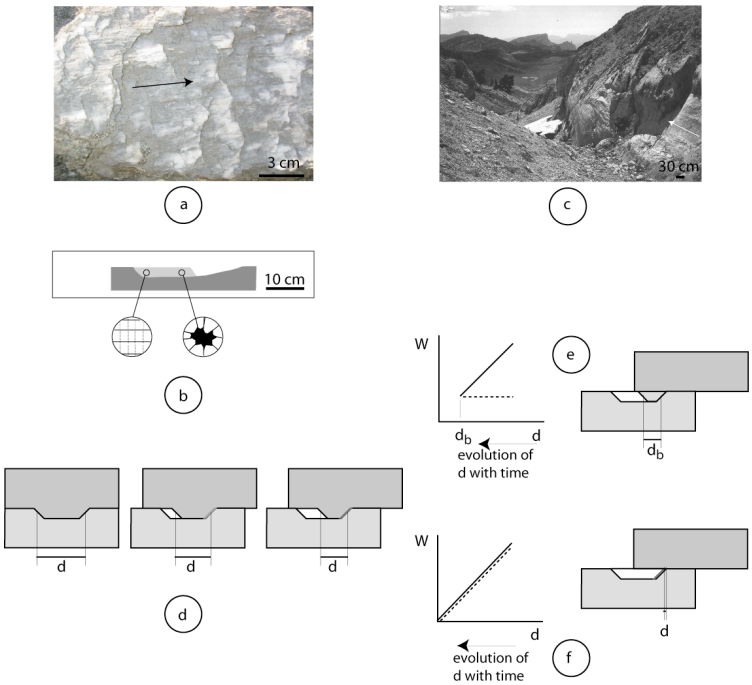

Figure 5

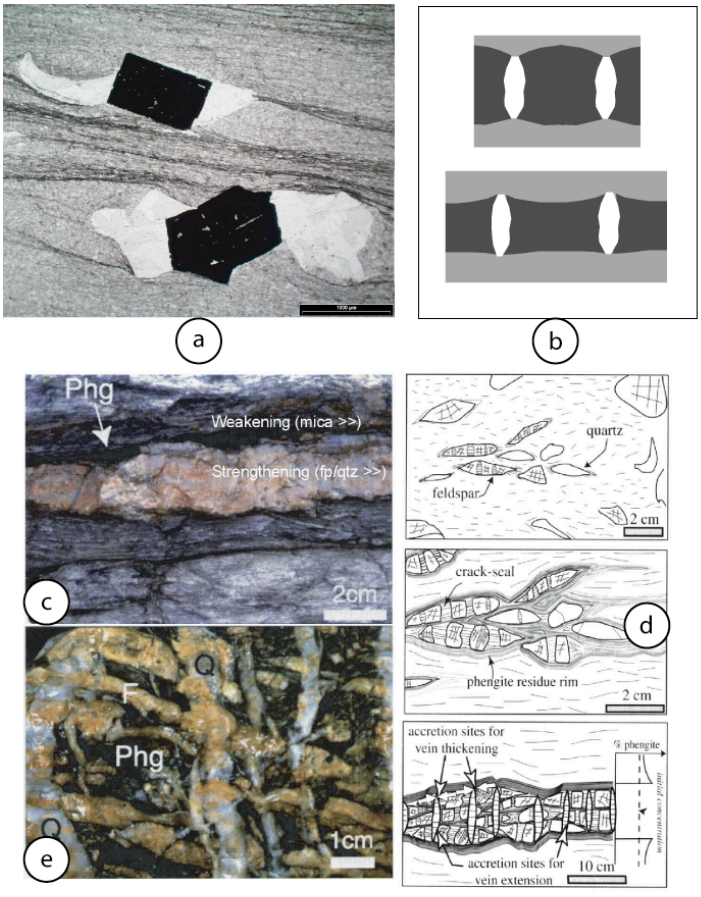

Gratier & Gueydan, Figure 6

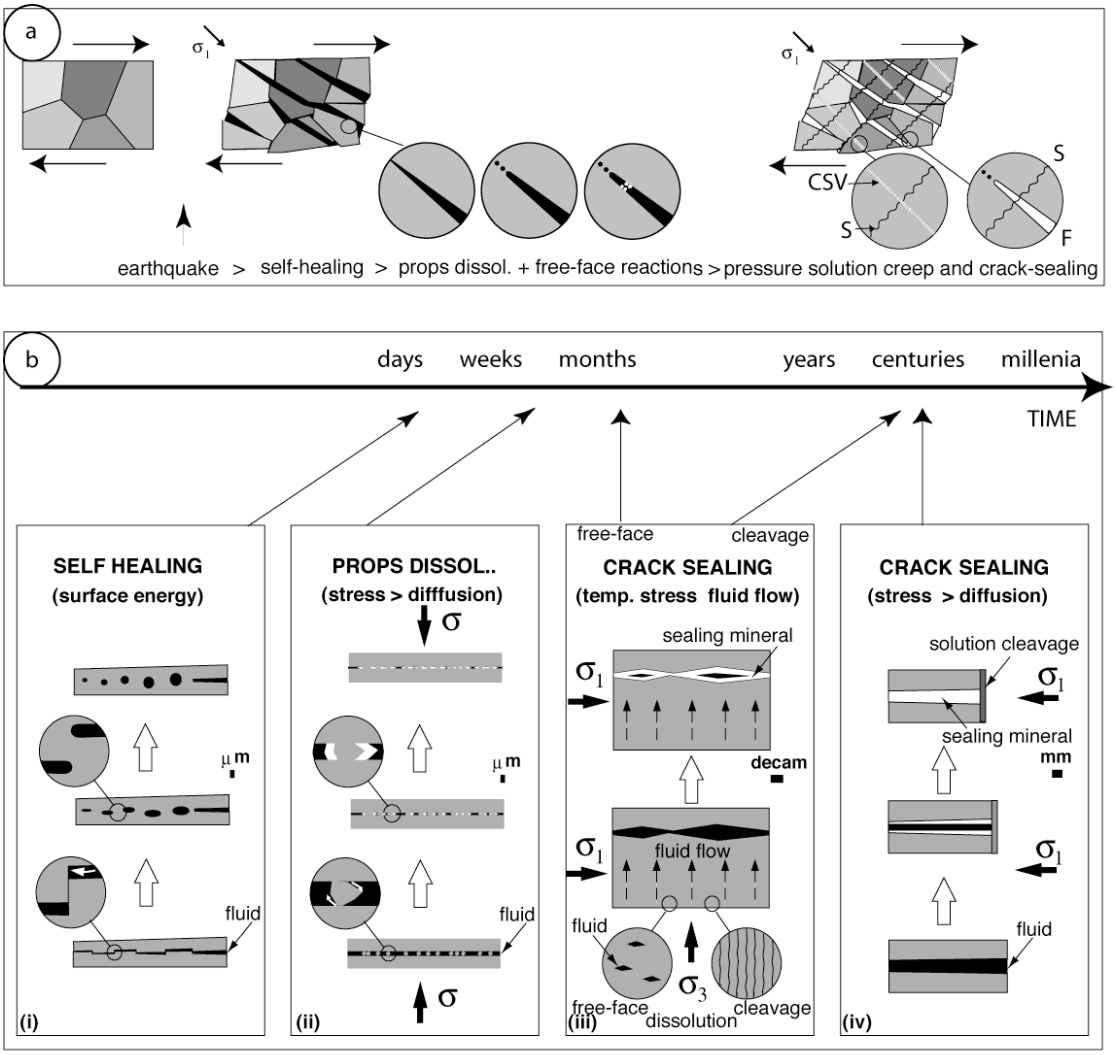
a
σ1
CSV
S
F
earthquake > self-healing > props dissol. + free-face reactions > pressure solution creep and crack-sealing
b
days
weeks
months
years
centuries
millenia
TIME
SELF HEALING
(surface energy)
μm
fluid
(i)
PROPS DISSOL..
(stress > difffusion)
σ
μm
fluid
σ
(ii)
free-face
cleavage
CRACK SEALING
(temp. stress fluid flow)
sealing mineral
σ1
decam
σ1
fluid flow
fluid
σ3
free-face
dissolution
cleavage
(iii)
CRACK SEALING
(stress > diffusion)
solution cleavage
σ1
sealing mineral
mm
σ1
fluid
(iv)

Figure 7

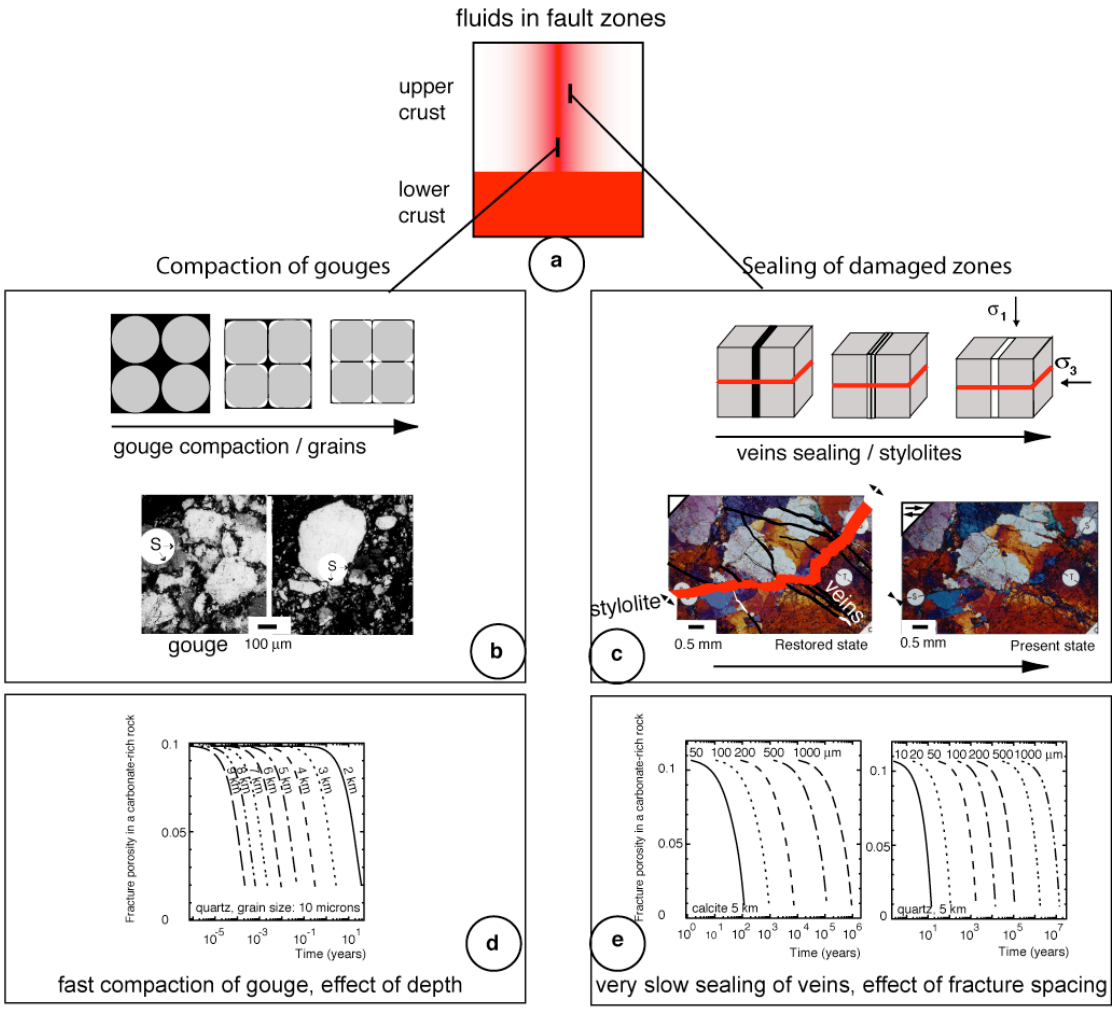
fluids in fault zones
upper crust
lower crust
a
Compaction of gouges
Sealing of damaged zones
gouge compaction / grains
gouge
100 µm
b
veins sealing / stylolites
stylolite
veins
0.5 mm
Restored state
0.5 mm
Present state
c
Fracture porosity in a carbonate-rich rock
quartz, grain size: 10 microns
Time (years)
d
fast compaction of gouge, effect of depth
calcite 5 km
quartz, 5 km
Time (years)
e
very slow sealing of veins, effect of fracture spacing

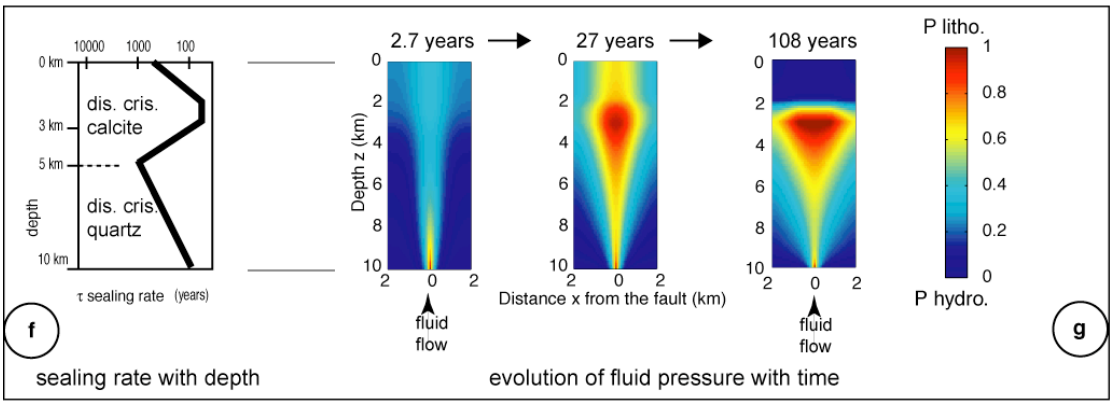
dis. cris. calcite
dis. cris. quartz
depth
τ sealing rate (years)
f
sealing rate with depth
2.7 years
27 years
108 years
Depth z (km)
Distance x from the fault (km)
fluid flow
P litho.
P hydro.
g
evolution of fluid pressure with time

Figure 8

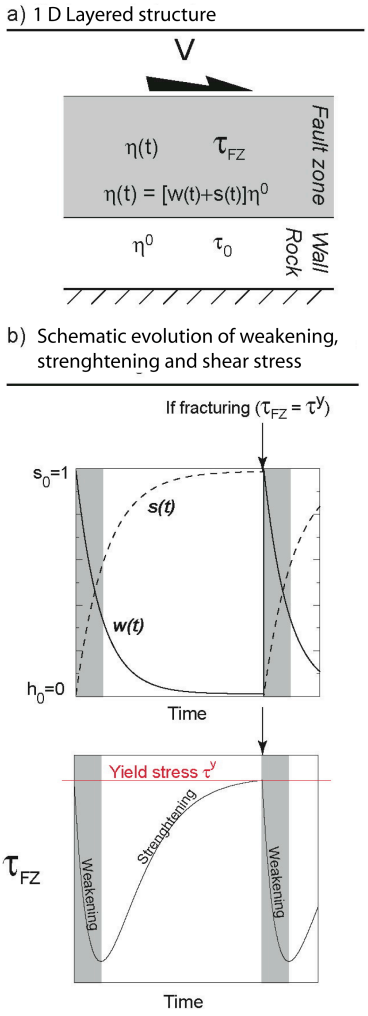

Gratier & Gueydan, Figure 9

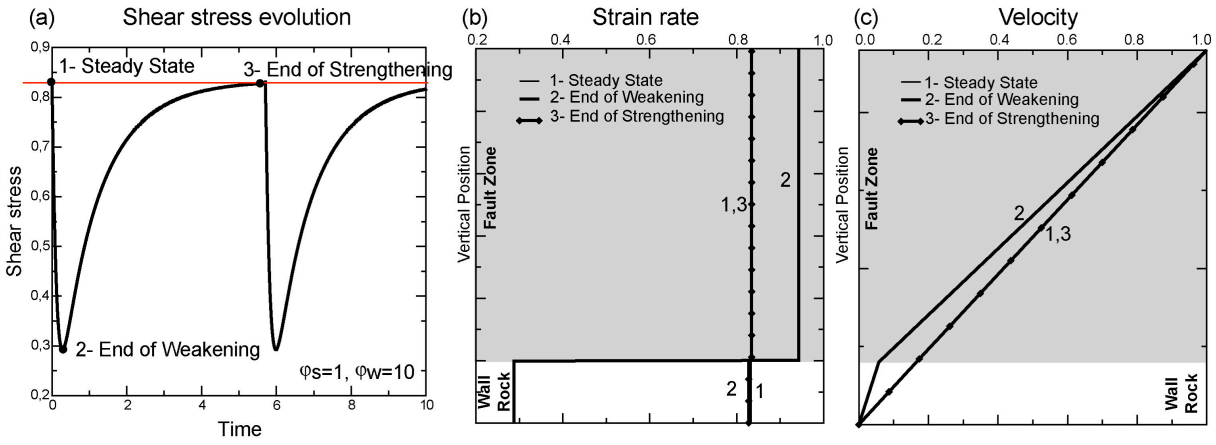

Gratier & Gueydan, Figure 10

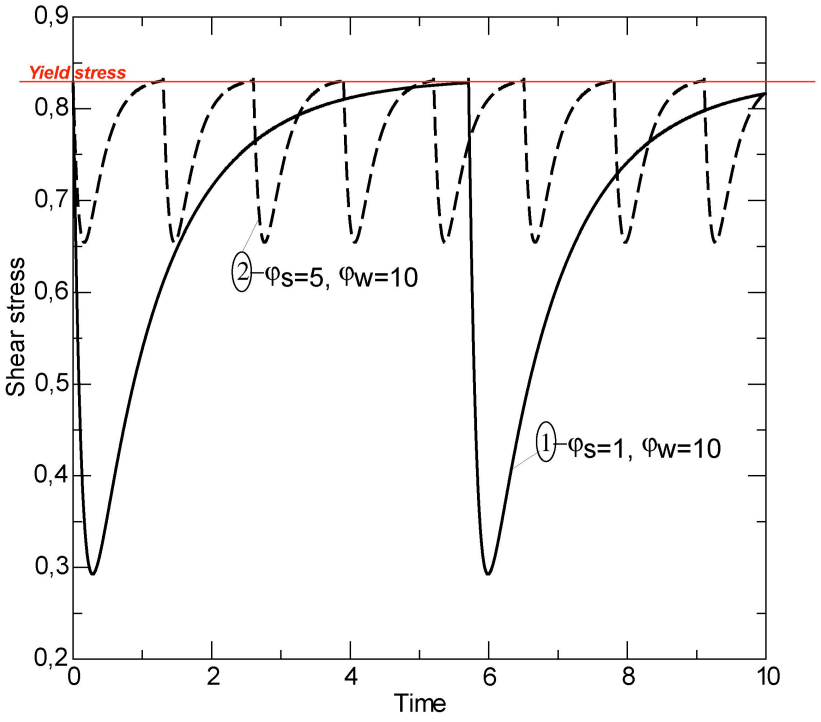

Gratier & Gueydan, Figure 11

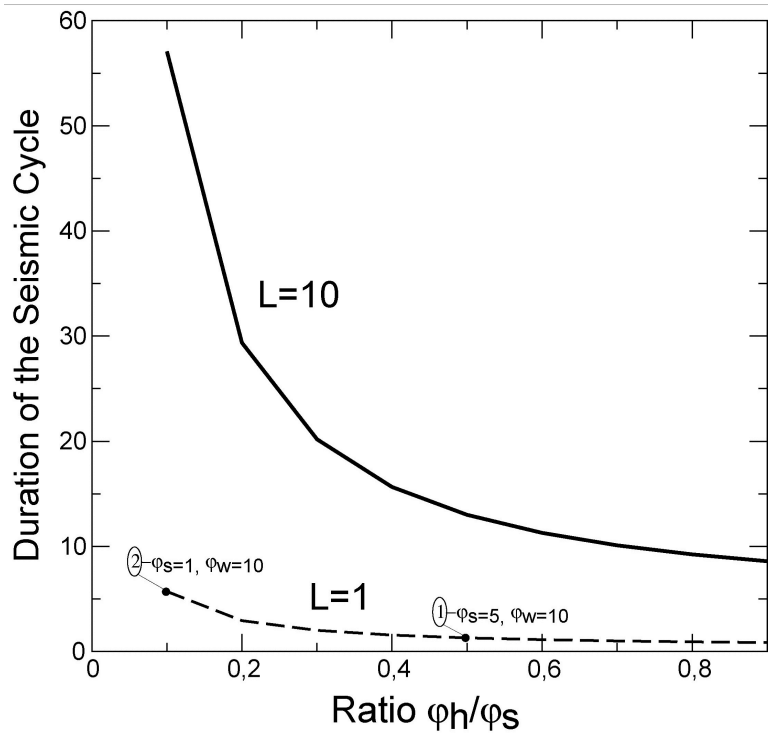

Gratier & Gueydan, Figure 12

FIGURES

Figure 1 *Schematic view of seismic and aseismic interactions in the crust. (a) Cataclastic, seismic faulting in the upper crust competes with aseismic deformation (folding, cleavage formation) associated with diffusive mass transfer (pressure solution, mineral reactions). In the lower crust, mostly aseismic deformation (predominantly by dislocation creep, diffusion creep) may be associated with rare earthquakes due to subordinate cataclasis. (b) Individual fault strands in the upper crust grow together to form mature fault zone networks during successive cycles (stars) and associated inflow of fluids and stress changes (τ). (c) Shear zone networks in the lower crust evolve over longer times, initially in a closed system for fluids. Coseismic ruptures propagate downward into the lower crust, creating pathways for the downward flow of fluids.*

Figure 2 *Basic concepts of pressure solution creep. (a) Dissolution at contact of fluid phases (continuous or discontinuous) with stressed solids (σ_1), the dissolved species are transferred by diffusion within this trapped fluid and re-deposited on the free surfaces of the solid at fluid pressure, P_f, or possibly on any surfaces that are in contact with the fluid and at a normal stress lower than σ_1. Various creep models are possible depending on the rate-limiting step of this process and on the mechanism of mass transfer: (b) diffusion along the boundaries of the solid driven by a chemical potential gradient; (c) fluid advection through the solid driven by head gradient $\Delta h/\Delta x$.*

Figure 3 *Drastic effect of fracturing on the kinetics of pressure solution creep. (a) The indenter experiment. (b) Displacement of indenter in halite with time: note drastic increase of the displacement-rate associated with radial fracturing (day 71); (c) Axial view (top) and cross sectional view (bottom) of the radial fractures that developed on day 71; (d) View of natural fractures at the contact between two stressed solids that underwent pressure-solution indenting. (e) The development of radial fractures reduces the mean distance of diffusive mass transfer within trapped fluids from d (before fracturing) to less than d/2 (after radial fracturing). (f) When diffusion is rate-limiting at a constant displacement-rate, increased surface of dissolution is counterbalanced by fracture development leading to unstable behaviour, adapted from Gratier et al. (1999).*

Figure 4 *Three examples of fracturing followed by fluid influx that triggered reaction-weakening and major strain localization within the lithosphere. Two examples are observed during extensional setting (upper part). At midcrustal depths, feldspar fracturing and reaction-softening (feldspar to mica transformation) lead to the formation of kilometre-scale shear zones, Tenda Massif, Corsica, (Gueydan et al., 2003). In the uppermost mantle, fracturing and hydrous phase transformations are coeval with the formation of ultramafic extensional shear zones (Handy and Stünitz, 2002). Localized deformation zones (a) and (b) define a mylonitic shear zone network that accommodates extension at depths, as depicted by Vissers et al. (1995). During continental subduction (lower part), seismic fracturing of granulites followed by fluid influx and eclogitisation facilitate strain localization (Austrheim and Boundy, 1994; Jolivet et al., in press). The exhumation of deep crustal units within the subduction channel may have occurred along the eclogitic shear zones.*

Figure 5 *Dissolution and fracturing of asperities along a fault. (a) Mineral fibers within voids created by the slow dissolution of asperities on a fault. (b) Detail of the process based on natural measurements showing the dissolution surface with directional roughness that opposes displacement on the fault: mineral fibers formed by successive crack-seal events (left) attesting to aseismic sliding that is controlled by the kinetics of pressure solution, another possibility is that cataclastic sliding was episodic as evidenced by some large openings that were sealed by euhedral crystals (right). (c) An exhumed fault surface showing the general threading of the fault parallel to the fault displacement (arrows) and the various asperities at all scales. (d) Schematic evolution of dissolution deposition at the scale of a single asperity; (e) Evolution of energy (W) needed to break (continuous line) or to dissolve (dotted lines dissolution models I or R, eq. 5 and 3) an asperity of decreasing size d; (f) Evolution of energy (W) needed to break (continuous line) or dissolve (dotted lines: dissolution model D, eq. 4) an asperity of decreasing size d, as adapted from Gratier and Gamond (1990).*

Figure 6 *Three examples of strengthening during high-strain deformation. (a) A pressure shadow that becomes stronger than the slaty matrix which it indented. (b) Quartz and calcite deposit between boudins (top) that becomes stronger than the boudin itself (bottom), as sketched from a natural example. (c to e) Examples from Porhyroïds units (Vendée, France) of fluid-assisted crack-seal deformation (Le Hebel et al., 2002): (c) The Porphyroïds are marked by alternating quartzo-feldspathic layers rimmed by phengitic layers; (d) Le Hebel et al. (2002) showed that this layering results from crack-sealing: with increasing strain pervasive fracturing of strong (qtz /fdp) layers is coeval with dissolution of feldspar and quartz in the matrix, leading to the development of phengitic residues. The K-rich fluids seal the numerous cracks, inducing*

growth of the quartzo-feldspathic layers; (e) Detailed view of the pervasive fracturing of the quartzo-feldspathic veins.

Figure 7 *(a) Schematic view of post-seismic sealing of a fault zone. The porosity (black) linked to the fracturing process is progressively sealed by mineral deposit (white). Dissolution along stylolites or solution cleavage (S) is triggered by fracturing (F) and is associated with aseismic post-seismic deformation that relaxes stress. Solution cleavage (S) and associated post seismic crack-seal veins (CSV) also accommodate part of the strain aseismically over the whole interseismic period. (b) The characteristic times of sealing vary from days to millennia, with self-healing driven by surface energy (i), dissolution of props driven by stress and a decrease in fluid pressure (ii), crack sealing with fluid infiltration controlled either by reactions on free-faces or by diffusion along solution cleavage (iii), crack sealing driven by stress with mass transfer from solution cleavage to fracture (iv). Figure adapted from Gratier et al. (2003).*

Figure 8 *(a) Fluids in the upper crust rising from depth along active faults as deduced from stable isotopes studies (Pili et al., 1998). (b – c) geometry of the compaction model (b) and crack sealing (c) deduced from observations of naturally compacted gouges (b) and fractures (c), as adapted from Gratier et al. (2003). Modelled effects of depth on gouge compaction (c) and of fracture spacing on sealing of fractures (c), as adapted from Renard et al. (2000). Post-seismic evolution of fluid pressure within fault (g) for predominantly calcite dissolution in the uppermost 5 km and dominantly quartz dissolution in the 5 to 10 km interval (f), with both crack sealing and fluid flow from depth, as adapted from Gratier et al. (2003).*

Figure 9 *(a) Depiction of the 1D layered model for the numerical simulation of strengthening and weakening during faulting. The layering (fault zone and wall rock) undergoes simple shearing at velocity V. The width of the fault zone is L. The viscosity of the wall rock is invariant with time, while the fault zone viscosity can change with time due to weakening w(t) and strengthening s(t). (b) Schematic evolution of the weakening and strengthening (top) and of shear stress (bottom) with time. Initially, weakening dominates (w > s), leading to a decrease in shear stress. Subsequently, strengthening prevails (s > w), loading the fault zone and leading up to renewed fracturing ($\tau_{FZ} \geq \tau^{y}$). Fracturing resets the weakening and strengthening to their initial values. See text for explanation.*

Figure 10: *(a) Shear stress variations with time (φ_s = 1and φ_w = 10). (b) Strain rate profiles and (c) velocity profiles in the fault zone and wall rock at the beginning of the earthquake cycle (point 1: steady state in a), at the end of the weakening (point 2 in a) and at the end of the strengthening (point 3 in a).*

Figure 11: *Shear stress variations with time for two rates of strengthening. The straight line (curve 1) was computed for φ_s = 1 and the dotted line (curve 2) for φ_s = 5. For these two curves, the rate of weakening is constant and set to φ_w = 10. Because $\varphi_w > \varphi_s$, weakening sets in immediately after fracturing ($\tau_{FZ} = \tau^{y}$, a condition drawn as the horizontal line labelled yield stress). Subsequently, strengthening dominates, leading to an increase in shear stress and ultimately triggering renewed fracturing. See text for explanation.*

Figure 12: *Duration of the earthquake cycle as a function of the ratio of strengthening to weakening rates for two values of the fault zone width, L. Points 1 and 2 refer to numerical simulation of Figure 10 for L = 1. See text for explanation.*

REFERENCES

Atkinson, B. K., 1982. Subcritical crack propagation in rocks: Theory, experimental results and applications, *J. Structural Geol*ogy, **4:** 41– 56.

Austrheim, H., Boundy, T., 1994 Pseudotachylites generated during seismic faulting and eclogitization of the deep crust, *Science*, **265:** 82-83.

Beeler, N.M., Hickman, S.H., 2004. Stress-induced, time-dependent fracture closure at hydrothermal conditions. *J. Geophysical Research* **109:** (B2*)* 1-16.

Blanpied, M L, Lockner, D A, Byerlee, J D, 1995. Frictional slip of granite at hydrothermal conditions, *J. Geophysical Research* **100:** (B7) 13045-13064.

Bokelmann, G.H.R., Kovach, R., 2003. Long-term creep rate changes and their causes. *Geophysical Research Letters*, **30** (8), NIL_9-NIL_12.

Bos, B., Peach, C.J., Spiers, C.J. , 2000. Frictional-viscous flow of simulated fault gouge caused by the combined effects of phyllosilicates and pressure solution, *Tectonophysics*, **327**: 173-194.

Brantley, S., Evans, B., Hickman, S.H., Crerar, D.A., 1990. Healing of microcracks in quartz: implications for fluid flow. *Geology,* **18**: 136-139.

Cosgrovbe, J.W., 1976. The formation of crenulation cleavage. *J. Geological Society London*, **132**: 155-178.

De Boer, R.B., Nagtegaal, P.J.C., Duyvus, E.M. 1977. Pressure solution experiment on quartz sand. *Geochimica Cosmochimica Acta,* **41:** 257-264.

de-Meer, S. Spiers, C.J., Peach, C.J., Watanabe, T., 2002 Diffusive properties of fluid-filled grain boundaries measured electrically during active pressure solution. *Earth and Planetary Science Letters*, **200:** (1-2) 147-157.

den Brok, S.B., 1998. Effect of microcracking on pressure-solution strain rate: the Gratz grain boundary model. *Geology*, **26**: 915-918.

Dewers, T., Ortoleva, P., 1990. A coupled reaction / transport / mechanical model for intergranular pressure solution stylolites, and differential compaction and cementation in clean sandstones. *Geochimica Cosmochimica Acta*, **54**: 1609-1625.

Dixon, J., Williams, G., 1983. Reaction softening in mylonites from the Arnaboll thrust, Sutherland, *Scott. J. Geology*, **19:** (2) 157-168.

Dysthe-DK; Renard, F., Feder, J., Jamtveit, B., Meakin, P., Jøssang T., 2003. High-resolution measurements of pressure solution creep. *Physical Review E*, **6801:** (1) 317-329.

Elias, B.P., Hajash, A., 1992. Changes in quartz solubility and porosity due to effective stress: An experimental investigation of pressure solution. *Geology*, **20**: 451-454.

Etheridge, M.A., Cox, S.F., Wall, V.J., Vernon, R.H. 1984. High fluid pressures during regional metamorphism and deformation: implication for mass transfer and deformation mechanisms, *J. Geophysical Research*, **89**: 4344-4558.

Evans, J.P., Chester, F.M., 1995. Fluid-rock interaction in faults of the San Andreas system: inference from the San Gabriel fault rock geochemistry, *J. Geophysical Research*, **100:** 13,007-13,020.

Farver, J.R., Yund, R.A., 1998. Oxygen grain boundary diffusion in natural and hot-pressed calcite aggregates. *Earth and Planetary Science Letters***, 161**: 189-200.

Fitz Gerald, J.D., H. Stünitz, 1993. Deformation of granitoids at low metamorphic grade. I: Reactions and grain size reduction, *Tectonophysics*, **221**: 269-297,.

Fletcher, R.C., Pollard, D.D., 1981. Anticrack model for pressure solution surfaces. *Geology*, **9**: 419-424.

Furlong, K., Beroza, G.C., Brun, J.-P., Cowie, P.A., Handy, M.R., Mooney, W.D., Taymaz, T., Teyssier, C., Vauchez, A., Wernicke B. Nucleation and Growth of Fault Systems, In: The Dynamics of Fault Zones, edited by M.R. Handy, G. Hirth, N. Hovius, Dahlem Workshop Report 95, The MIT Press, Cambridge, Mass., USA

Fyfe, W.S., Price, N.J., Thomson, A.B. 1978. Fluids in the earth's crust, Development in geochemistry, Elsevier, Amsterdam.

Gapais, D., 1989. Shear structures within deformed granites: Mechanical and thermal indicators, *Geology*, **17:** 1144-1147.

Gibbs, J.W., 1877. On the equilibrium of heterogeneous substances. *Transaction of the Connecticut Academy*, **3:** 108-248, 343-524.

Gratier, J.P., 1987. Pressure solution-deposition creep and associated tectonic differentiation in sedimentary rocks. In: M.E. Jones and R.M.F. Preston (Editors), Deformation of Sediments and Sedimentary Rocks. *Geological Society London Special Publication*, **29:** 25-38.

Gratier, J.P., Gamond, J.F., 1990. Transition between seismic and aseismic deformation in the upper crust. In: R.J. Knipe and E.H. Rutter (Editors), Deformation mechanisms, rheology and tectonics. *Geological Society London Special Publication*, **54:** 461-473.

Gratier, J.P., Renard, F., Labaume, P., 1999. How pressure-solution and fractures interact in the upper crust to make it behave in both a brittle and viscous manner. *J. Structural Geology*, **21**: 1189-1197.

Gratier, J.P., Favreau, P., Renard, F., 2003. Modeling fluid transfer along California faults when integrating pressure solution crack sealing and compaction processes. *J. Geophysical Research*, **108**: (B2): 28-52.

Gratz A.J., 1991. Solution-transfer compaction of quartzites: Progress toward a rate law. *Geology,* **19**: 901-904.

Gueydan, F., Leroy, Y.M., Jolivet, L., Agard, P. 2003. Analysis of continental midcrustal strain localization induced by reaction-softening and microfracturing, *J. Geophysical Research* **108**: (B2), 2064, doi:10.1029/2001JB000611.

Handy, M.R. 1989 Deformation regime and the rheological evolution of fault zones in the lithosphere. The effect of pressure, temperature, grain size and time, *Tectonophysics* **163:** *119-159.*

Handy, M.R., Stünitz, H. 2002. Strain localization by fracturing and reaction weakening- a mechanism for initiating exhumation of subcontinental mantle beneath rifted margins, in *Deformation Mechanisms, Rheology and Tectonics: Current Status and Future Perspectives*, edited by S. de Meer, M.R. Drury, J.H.P. de Bresser, and G.M. Pennock, *Geological Society, London, Special Publications* **200:** 387-407.

Handy, M.R., Hirth, G., Bürgmann, R. 2005. Continental Fault Structure and Rheology from the Frictional-to-Viscous Transition Downwards, In: The Dynamics of Fault Zones, edited by M.R. Handy, G. Hirth, N. Hovius, Dahlem Workshop Report 95, The MIT Press, Cambridge, Mass., USA

Hickman, S.H., Evans, B., 1991. Experimental pressure solution in halite: the effect of grain/ interphase boundary structure. *J. Geological Society London*, **148:** 549-560.

Hickman, S., Sibson, R.H., Bruhn, R., 1995. Introduction to special section: Mechanical involvement of fluids in faulting. *J. Geophysical Research*, **100**: (B7) 12831-12840.

Hickman, S.H., Evans, B., 1995. Kinetics of pressure solution at halite-silica interfaces and intergranular clay films, *J. Geophysical Research,* **100**: B7, 13113-13132.

Hilgers, C., Dilg-Gruschinski, K., Urai, J.L., 2004. Microstructural evolution of syntaxial veins formed by advective flow. *Geology,* **32**: (3) 261-264.

Jolivet, L., Raimbourg, H., Labrousse, L., Avigad, D., Leroy, Y.M., Austrheim, H.. Andersen, T.B Softening trigerred by eclogitisation, the first step toward exhumation during continental subduction, *Earth and Planetary Science Letters*, in press.

Kennedy, B.M., Kharaka, Y.K., Evans, W.C., Ellwood, A., DePaolo, D.J., Thordsen, J., Ambats, G. Mariner. R.H., 1997. Mantle fluids in the San Andreas fault system, California, *Science,* **278,** 1278-1280.

Kingery, W.D., Bowen, H.K., Uhlmann, D.R., 1976. Introdcution to ceramics, John Wiley & Sons, 1032p.

Klaper, E. M. 1990. Reaction-enhanced formation of eclogite-facies shear zones in granulite-facies anorthosites. In Deformation mechanisms, rheology and tectonics (eds R.J.Knipe and E.H.Rutter), *Geological Society London, Special Publication*, **54**, 167–74.

Knipe, R.J., Wintsch, R.P. 1985. Heterogeneous deformation, foliation development, and metamorphic processes in a polyphase mylonite. In: Thompson AB, Rubie DC (eds) Metamorphic reactions: kinetics textures, and deformation. Springer, Berlin Heidelberg New York, pp 180–210.

Le Hebel, F., Gapais, D., Fourcade, S., Capdevila, R., 2002. Fluid-assisted large strains in a crustal-scale décollement (Hercynian Belt of South Brittany, France), in *Deformation Mechanisms, Rheology and Tectonics: Current Status and Future Perspectives*, edited by S. de Meer, M.R. Drury, J.H.P. de Bresser, and G.M. Pennock, *Geological Society, London, Special Publications,* **200:** 85-101.

Lehner, F.K. 1995. A model for intergranular pressure solution in open systems, *Tectonophysics,* **245***: 153-170.*

Li, Y.G., Vidale, J.E., 2001. Healing of the shallow fault zone from 1994-1998 after the 1992 M7.5 Landers, California, earthquake. *Geophysical Research Letters*, **28:** (15) 2999-3002.

Li, Y.G., Vidale, J.E., Day, S.M., Oglesby, D.D., Cochran, E., 2003. Postseismic fault healing on the rupture zone of the 1999 M 7.1 Hector Mine, California, earthquake. *Bull. Seismological Society America*, **93:** (2) 854-869.

McEwen, T.J. 1978. Diffusional mass transfer processes in pitted pebble conglomerates, *Contribution Mineralogy Petrology* **67:** 405-415.

Means, W.D., Li, T., 2001. A laboratory simulation of fibrous veins: some first observations. *J. Structural Geology,* **23**: (6-7) 857-863.

Miller, S.A. , 2002. Properties of large ruptures and the dynamical influence of fluids on earthquakes and faulting, *J. Geophysical Research*, **107**: 536-548.

Miller, S.A., van-der-Zee, W., Olgaard, D.L., Connolly, J.A.D., 2003. A fluid-pressure feedback model of dehydration reactions: experiments, modelling, and application to subduction zones, *Tectonophysics,* **370:** 241-251.

Mitra, G., 1978. Ductile deformation zones and mylonites: the mechanical process involved in the deformation of crystalline basement rocks, *American J. Science*, **278:** 1057-1084.

Muhuri, S.K., Dewers, T.A., Scott, G.E., Reches, Z., 2003. Interseismic fault strenghtening and earthquake-slip instability: friction or cohesion. *Geology,* **31:** (10) 881-884.

Muller, W., Aerden, D., Halliday, A.N., 2000. Isotopic dating of strain fringe increments: duration and rates of deformation, in shear zones, *Science,* **288:** 2195-2197.

Nadeau, R.M., Johnson, L.R., 1998. Seismological Studies at Parkfield VI: Moment Release Rates and Estimates of Source Parameters for Small Repeating Earthquakes. *Bull. Seismological Society America*, **88:** 790-814.

Niemeijer, A.R., Spiers, C.J., 2002. Compaction creep of quartz sand at 400-600°C: experimental evidence for dissolution controlled pressure solution. *Earth and Planetary Science letters*, **195**: 261-273.

Oelkers, E.H., Bjørkum, P.A., Murphy, W.M., 1996. A petrographic and computational investigation of quartz cementation and porosity reduction in North Sea sandstones. *American Journal of Science*, **296:** 420-452.

Paterson, M.S., 1973. Nonhydrostatic thermodynamics and its geologic applications. *Reviews of Geophysics and Space Physics*, **11:** 355-389.

Paterson, M.S., 2001. Relating experimental and geological rheology, *International J. Earth Sciences (Geol. Rundsch)***, 90**: 157-167.

Person, M. L., Baumgartner, P., Bos, B., Connolly, J., Gratier, J.P., Gueydan, F., Miller, S.A., Rosenberg, C.L., Urai, J., Yardley B.W.D. 2005. Fluids, Geochemical Cycles, and Mass Transport in Fault Zones, In: The Dynamics of Fault Zones, edited by M.R. Handy, G. Hirth, N. Hovius, Dahlem Workshop Report 95, The MIT Press, Cambridge, Mass., USA

Pfiffner, O.A., Ramsay, J.G. 1982. Constraints on geological rate: arguments from finite strain values of naturally deformed rocks. *J. Geophysical Research*, **87**, 311-321.

Pili, E.B., Kennedy, B.M., Conrad, M.S., Gratier, J.P. 1998. Isotope constraints on the involvmenbt of fluids in the San Andreas fault, *Eos Trans. AGU*, **79**(17): S229-S320, Spring meeting

Raj, R., 1982. Creep in polycrystalline aggregates by matter transport through a liquid phase. *J. Geophysical Research*, **87:** 4731-4739.

Ramsay, J.G., 1980. The crack-seal mechanism of rock deformation. *Nature*, **284:** 135-139.

Renard, F., Park, A., Gratier, J.P., Ortoleva, P., 1997. An integrated model for transitional pressure solution in sandstone, *Tectonophysics,* **312:** 97-115.

Renard, F., Gratier, J.P., Jamtveit, B., 2000. Kinetics of crack-sealing, intergranular pressure solution and compaction around active faults, *J. Structural Geology*, **22:** 1395-1407.

Robin, P.Y. 1978. Pressure solution at grain to grain contacts, *Geochimica Geochimica Acta***, 42**: 1383-1389.

Robin, P.Y. 1979. Theory of metamorphic segregation and related processes, *Geochimica et Cosmochimica Acta,* 43, 1587-1600.

Rutter, E.H., 1976. The kinetics of rock deformation by pressure solution. *Philosophical Transactions of the Royal Society of London*, **283:** 203-219.

Rutter, E.H., 1983. Pressure solution in nature, theory and experiment, *J. Geological Society London.* **140**: 725-740.

Sammis, G.C., Rice, J.R., 1998. Repeating earthquakes as low-stress-drop events at a border between locked and creepng fault patches. *Bull. Seismological Society America*, **91:** 532-537.

SARPP, 2003 Structural Analysis and Rock Physics Program, Y. M. Leroy and F. Gueydan, LMS, Ecole Polytechnique, Palaiseau, France.

Shimizu, I. 1995. Kinetics of pressure solution creep in quartz: theoretical consideration, *Tectonophysics***, 245**: 121-134.

Sibson, R.H., Robert, F., Poulsen, H.H.A.F. 1988. High Angle Faults, Fluid Pressure Cycling and Mesothermal Gold-Quartz Deposits. *Geology,* **16**: 551-555.

Sibson, R.H., Rowland, J.V., 2003. Stress, fluid pressure and structural permeability in seismogenic crust, North Island,

New Zealand, *Geophysical International Journal*, **154**: 584-594.

Simpson, C., 1985. Deformation of granitic rocks across the brittle-ductile transition, *J. Structural Geology,* **7**: (5), 503-511.

Sorby, H.C. (1865) On impressed limestone pebbles, as illustrating a. new principle in chemical geology. *Proc. West Yorks Geological Society,* **14**: 458–461.

Spiers, C.J., Schutjens, P.M., 1990. Densification of crystalline aggregates by fluid phase diffusional creep. In: D.J. Barber and P.G. Meredith (Editors), Deformation process in minerals, ceramics and rocks. Unwin Hyman, pp. 334-353.

Stel, H. 1981. Crystal growth in cataclasites: Diagnostic microstructures and implications. *Tectonophysics,* 78, 585-600.

Taber, S., 1916. The growth of crystals under external pressure. *American Journal of Science*, XLI (4Th Series), **246:** 532-556.

Tada, R., Siever, R. 1986. Experimental knife-edge pressure solution of halite, *Geochimica et Cosmochimica Acta,* **50**: 29-36.

Tenthorey, E., Cox, S.F., Todd, H.F., 2003. Evolution of strength recovery and permeability during fluid-rock reaction in experimental fault zones. *Earth and Planetary Science Letters*, **206:** (1-2) 161-172.

Thibaut, M., Gratier, J.P., Léger, M., Morvan, J.M., 1996. An inverse method for determining three dimentional fault geometry with thread criterion: application to stike-slip and thrust faults (Western Alps and California). *J. Structural Geology*, **18:** 1127-1138.

Tullis, T.E., Burgmann, R., Cocco, M., Hirth, G., King, G., Oncken, O. Otsuki, K. Rice, J.R., Rubin, A., Segall, P. Shapiro, S., Wibberley, C.A.J., 2005. Rheology of fault rocks and their suroundings, In: The Dynamics of Fault Zones, edited by M.R. Handy, G. Hirth, N. Hovius, Dahlem Workshop Report 95, The MIT Press, Cambridge, Mass., USA.

Vissers, R.L.M., Platt, J.P., van der Wal, D., 1995. Late orogenic extension of the Betic Cordillera and the Alboran Domain: a lithospheric view. *Tectonics,* **14:** 786-803.

Weyl, P.K., 1959. Pressure solution and the force of crystallization: a phenomenological theory. *J. Geophysical Research*, **64:** 2001-2025.

White, S.H., Knipe, R.J., 1978. Transformation and reaction-enhanced ductility in rocks, *J. Geological Society London*, **135:** 513-516.

Wibberley, C.A.J., 1999. Are feldspar-to-mica reactions necessarily reaction-softening process in fault zones, *J. Structural Geology*, **21:** 1219-1227.

Wintsch, R.P., Christoffersen, R., Kronenberg, A.K. (1995) Fluid-rock reaction weakening in fault zones, *J. Geophysical Research*, **100**: 13,021-13,032.

Yardley, B.W.D., Baumgartner, L.P. 2005. Fluid processes in deep crustal fault zones, In: The Dynamics of Fault Zones, edited by M.R. Handy, G. Hirth, N. Hovius, Dahlem Workshop Report 95, The MIT Press, Cambridge, Mass., USA.

Zhang, X., Salemans, J., Peach, C.J., Spizers, C.J., 2002. Compaction experiments on wet calcite powder at room temperature: evidence for operation of intergranular pressure solution. In Deformation mechanisms, rheology and tectonics: current status and furture perspectives, S. de Meer, M.R. Drury, J.H.P. de Bresser & J.M. Pennock eds, *Geological Society of London, Special Publication* **200:** 29-40.

Zubtsov, S.F., Renard, F., Gratier, J.P., Guiguet, R., Dysthe, D.K., Traskine, V.Y., 2004. Experimental pressure solution creep of polymineralic aggregates. *Tectonophysics*, **385**: 45-47.